WSRC-STI-2007-00544, Rev. 2

# Conceptual Model of Waste Release from the Contaminated Zone of Closed Radioactive Waste Tanks

**M. E. Denham**

**November 2010**

Savannah River National Laboratory
Savannah River Nuclear Solutions
Aiken, SC 29808

**Prepared for the U.S. Department of Energy Under Contract Number DE-AC09-08SR22470**

SRNL
SAVANNAH RIVER NATIONAL LABORATORY

## Reviews and Approvals

**Author**

M.E. Denham, Environmental Science & Biotechnology — Date: 11-16-2010

**Technical Reviewer**

L.A. Bagwell, Environmental Science & Biotechnology — Date: 16 NOV 2010

**L3 Manager**

R.S. Aylward, Environmental Science & Biotechnology — Date: 11/16/10

## Disclaimer



**Printed in the United States of America**

**Prepared For**
**U.S. Department of Energy**

**Table of Contents**

**List of Figures**

**List of Tables**

# Waste Release Conceptual Model

A fundamental part of estimating and understanding the eventual release of contaminants from closed waste tanks is a good conceptual model of contaminant leaching from residual waste. This document poses a realistic conceptual model followed by an achievable method of implementing the conceptual model in the framework of a flow and transport model. The simplifications that allow implementation of the conceptual model are documented and justified. In the most general sense, the model assumes that the residual waste remains as a discrete layer at the bottom of the tanks after they are filled with reducing grout. Henceforth, this discrete layer is referred to as the contaminated zone and abbreviated CZ. Infiltration from the surface or groundwater that passes through the tanks provides the pore fluids necessary to leach contaminants from the CZ.

Previous models of tank closure performance have used a constant leach rate for contaminant release from the CZ. This is unrealistic because conditions within the tanks will evolve over the period of interest and leaching of radionuclides from the CZ depends on the chemical composition of pore fluid passing through the zone. Adsorption and solubility of all of the radionuclides of concern vary with pH, and most vary with redox potential as well. Other parameters, such as carbonate concentration, can also affect the leaching of some of the radionuclides. As the grout filled tanks age, chemical composition of the pore fluid passing through the tanks will change resulting in changes to the solubility and adsorption controls on contaminant release.

Most of the tanks do not contact the water table and are referred to here as non-submerged. For these tanks the conceptual model of radionuclide leaching from the CZ divides the tank evolution into four potential conditions shown schematically in Figure 1.

Condition 1: Commences immediately following pouring of grout. The steel tank liner is assumed to be intact. It is assumed that pore fluids in the CZ that remain after washing are squeezed upward into the grout. No contaminants are released from the tank.

Condition 2: Commences when steel tank liner is breached, if infiltration flow is predominantly along preferential flow paths. The assumption is that initially the tank grout will be too impermeable to allow significant advective flow, so flow along preferential paths will dominate. These paths could be at the interface of the grout and the steel tank liner or the grout and tank infrastructure such as piping. It is assumed that the reducing capacity of the grout along these preferential flow paths is rapidly depleted. Thus, conditions of fluid reaching the CZ in this condition are relatively oxidizing.

Condition 3: Commences when general advective flow becomes dominant over flow along preferential pathways. For this conceptual model, general advective flow is defined as flow through a porous medium or along a fracture network extensive enough to be considered homogeneous on the scale of the tanks. If this is the case when the steel tank liner is breached, then Condition 2 does not occur, and the tank evolution proceeds to Condition 3. It is assumed that general advective flow through the reducing grout will produce reducing conditions in the pore water passing through the CZ.

Condition 4: Commences when reducing capacity of the tank grout is exhausted. In this condition, general advective flow dominates and pore water passing through the CZ is relatively oxidizing.

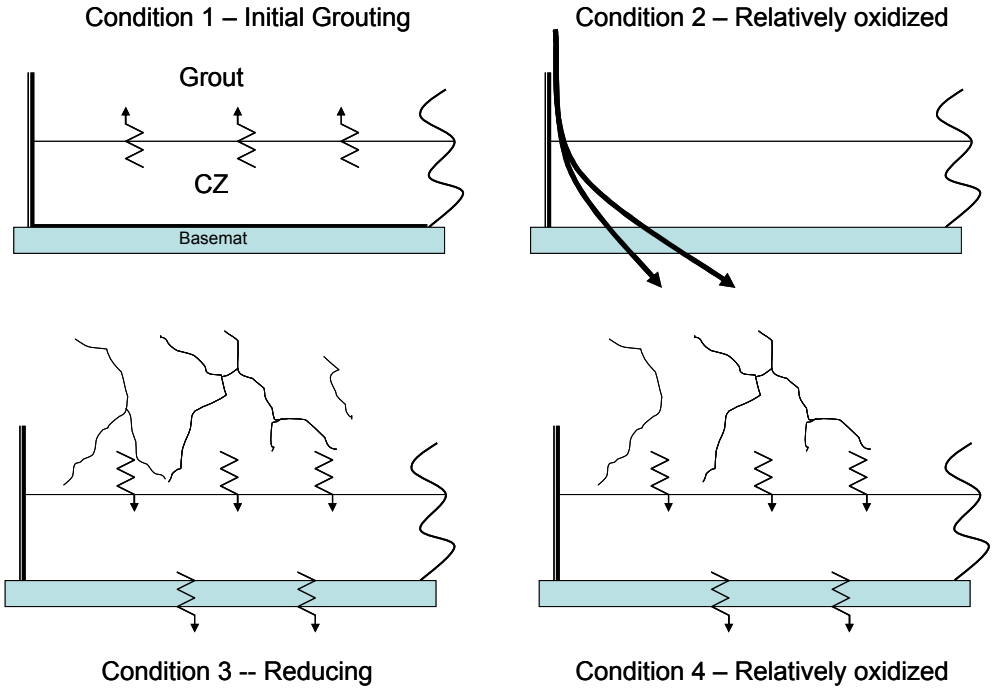


**Figure 1: Potential physical conditions of closed tanks in conceptual model.**

These conditions only reflect changes in redox potential of the pore fluids. The pH of the pore fluids will also evolve as the tanks age. Bradbury and Sarott (1995) described evolution of pore fluid pH in cementitious waste forms in three regions, of which the latter two are pertinent to this conceptual model. They assumed that cement in Region II had pore fluids in equilibrium with portlandite ($Ca(OH)_2$) and a pH above 12. However, the reducing grout to be used in tank closure will not have free portlandite at full hydration. Rather, the hydrated calcium silicate gel (CSH) will control pH at approximately 11.1. Eventually, the grout becomes fully carbonated and evolves to Region III in which pore fluids are in equilibrium with calcite ($CaCO_3$) and have a pH near 8.

The conceptual model that emerges from this multi-condition approach will result in a non-uniform leaching rate that depends on the chemical state of pore fluid contacting the waste at any given time. To allow maximum flexibility the waste release conceptual model addresses four chemical states, shown in Table 1, and the corresponding tank conditions that are represented by these four states. The chemical states do not apply to Condition 1 because the tank liner is intact and there is no fluid flow through the CZ.

**Table 1: Chemical states of the tanks and the tank condition to which they correspond.**

| Chemical State | Tank Condition |
|---|---|
| Oxidizing Region II | 2 and 4, CSH dominant |
| Oxidizing Region III | 2 and 4, calcite dominant |
| Reducing Region II | 3, CSH dominant |
| Reducing Region III | 3, calcite dominant |

There are a few tanks in H-Area in which the CZ is currently below or very close to the water table (Hamm and Collard, 2010). Groundwater could influence the solubility of radionuclides in these tanks when the tank liner fails. For this to occur lateral flow of groundwater through the tank would have to predominate over vertical flow of infiltrate. To evaluate the potential influence of groundwater on radionuclide solubility, four different chemical conditions were simulated that show varying degrees of groundwater influence. The basis for these is shown in Figure 2. The groundwater composition used is from a background water table well, designated P27D (Strom and Kaback, 1992), approximately 450 meters east of Tank 43.

Condition A: Groundwater flows laterally directly into the CZ with no effect of outer concrete.

Condition B: Groundwater equilibrates with outer concrete before passing through the CZ

Condition C: Groundwater flows laterally directly into the CZ with no effect of outer concrete and mixes with a small amount of Reducing Region II grout pore fluid

Condition D: Groundwater flows laterally directly into the CZ with no effect of outer concrete and mixes with a small amount of Oxidizing Region II grout pore fluid

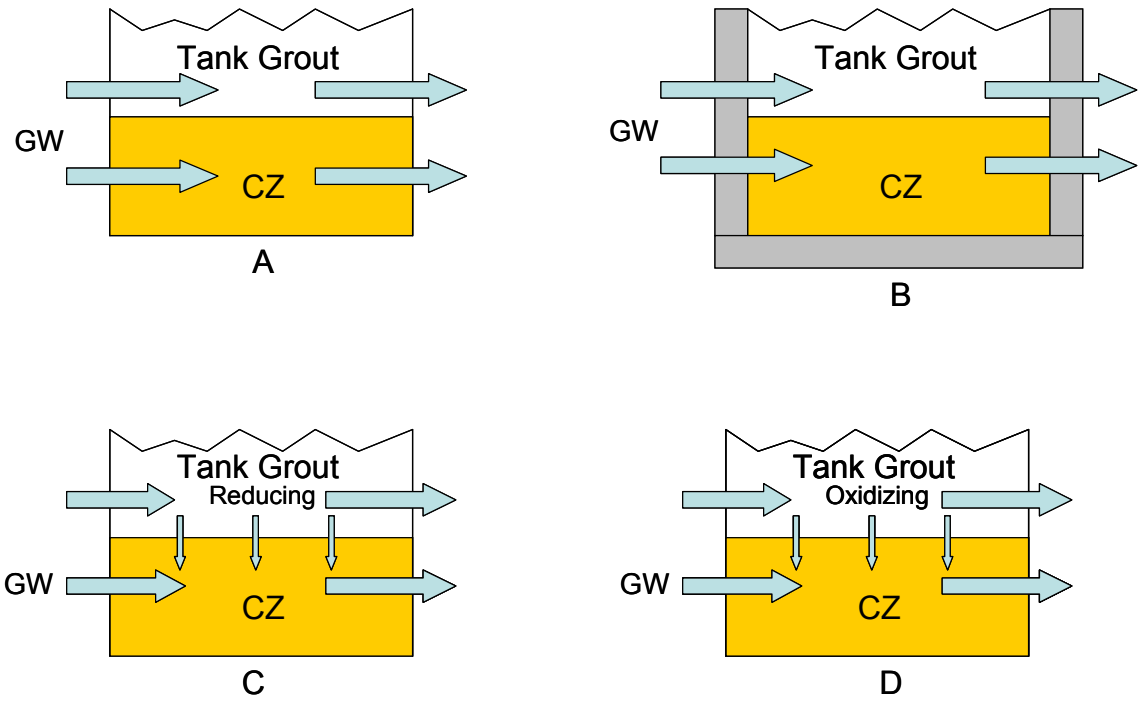


**Figure 2: Basis for four conditions controlling pore fluid chemistry in CZ of partially submerged tanks.**

In the waste release conceptual model there are three types of phases considered – an aqueous pore fluid phase, a matrix phase composed mostly of non-radionuclide elements, and discrete radionuclide phases embedded in the matrix. Each radionuclide is partitioned between the aqueous pore fluid, the surfaces of matrix phases in an adsorbed state, and discrete radionuclide phases. As long as the concentration of a radionuclide dissolved in the aqueous phase equals the solubility limit, release of that radionuclide is solubility controlled. Thus, as long as there are discrete particles of a radionuclide present, the rate of that radionuclide release is controlled by the flux of water through the CZ and the solubility of the discrete phase. If enough water passes through the CZ, the discrete phases of a particular radionuclide will be completely removed by dissolution and control of waste release will be by desorption from the surface of the matrix phases. Hence, adsorption controls only dominate the waste release when the mass of contaminant is insufficient to exceed the adsorption capacity of the non-radionuclide matrix phases. This can occur at any point during waste release, depending upon the inventory of a radionuclide and the adsorption capacity of the matrix. From that point on adsorption dominates waste release. Figure 3 shows this aspect of the waste release conceptual model.

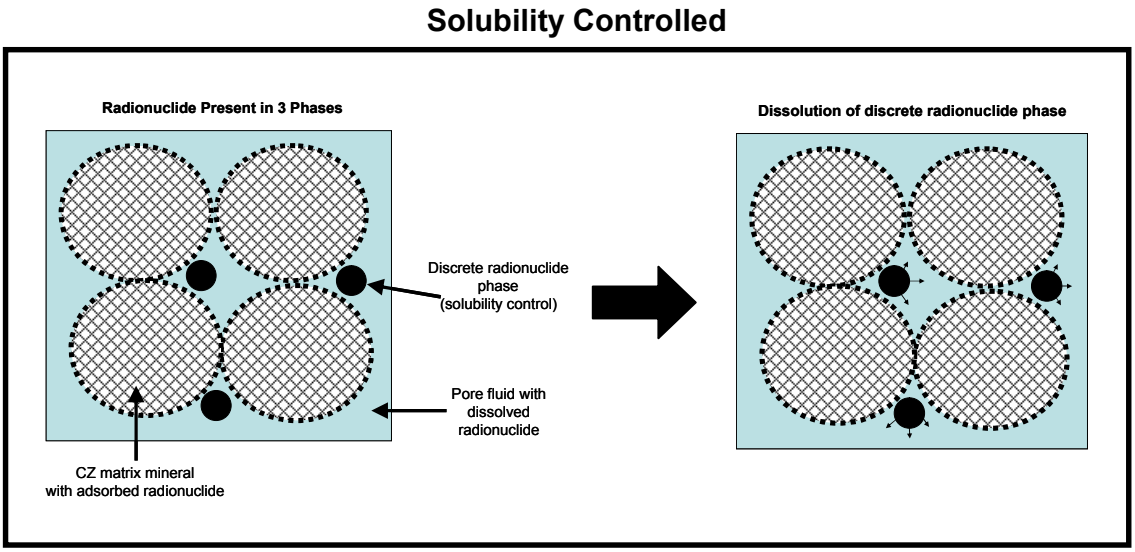


A)

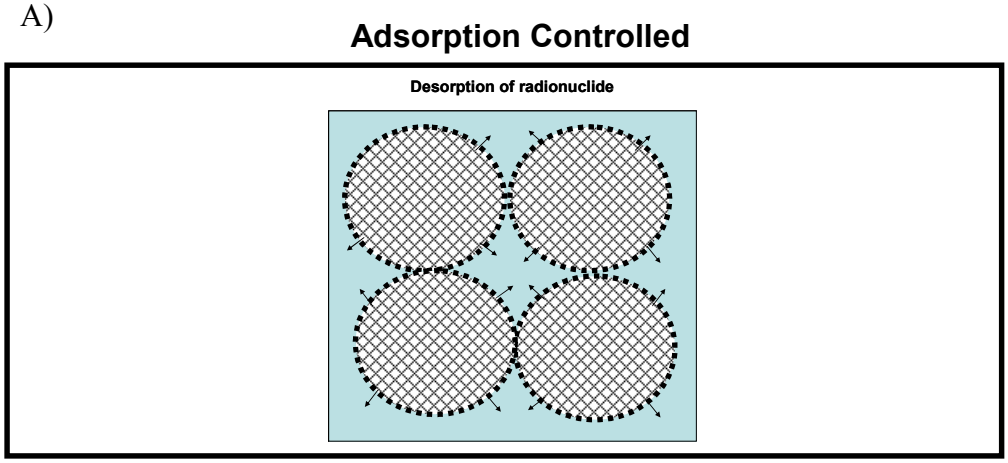


B)

**Figure 3: States of waste release – A) solubility controlled, B) adsorption controlled when discrete radionuclide phases are depleted.**

# Implementation of Conceptual Model

## *Solubility Calculations*

The first step in calculation of radionuclide solubilities was to estimate the chemical conditions associated with each chemical state listed in Table 1 and the four conditions of the partially submerged tanks. Simulations using the geochemical modeling program The Geochemist's Workbench®(Bethke, 2005) provided the degradation path of tank reducing grout, and hence the pore fluid composition of each condition in the conceptual model. The grout degradation simulations are briefly described in a later section and in more detail in Appendix B.

For the non-submerged tanks the pore fluid in the CZ at any given time is the pore fluid that has passed through the tank grout. Table 2 shows composition of pore water estimated for each of the chemical states listed in Table 1. Establishing the pore water composition of the four states allows solubilities for each radionuclide to be calculated by equilibrating a selected radionuclide phase with the pore water for each state. A total sulfur concentration of $1x10^{-5}$ molar (equivalent to 1mg/L $SO_4^{-2}$) was added to the pore fluids to be equilibrated with various solubility controlling radionuclide phases. This is a reasonable concentration based on the fact that at pH=12 equilibrium of the common cement phase ettringite [$Ca_6Al_2O_6(SO_4)_3 \cdot 32H_2O$] with C4AH13 [$Ca_4Al_2O_7 \cdot 13H_2O$] produces a sulfate concentration of 3 mg/L.

**Table 2: Chemical composition of pore water in each of the chemical states listed in Table 1.**

| Chemical State | pH | Eh(v) | $Ca^{+2}$ (molar) | $CO_3^{-2}$(molar) |
|---|---|---|---|---|
| Oxidizing Region II | 11.13 | 0.58 | $3.2x10^{-3}$ | $3.5x10^{-8}$ |
| Oxidizing Region III | 8.23 | 0.73 | $4.6x10^{-4}$ | $1.7x10^{-6}$ |
| Reducing Region II | 11.12 | -0.48 | $3.33x10^{-3}$ | $3.45x10^{-8}$ |
| Reducing Region III | 8.23 | -0.34 | $4.6x10^{-4}$ | $2.4x10^{-3}$ |

For the submerged tanks the pore fluid compositions in the CZ at any time are dictated by mixtures of groundwater and pore fluid passing from the tank grout into the CZ. Conditions A and B involve groundwater and groundwater equilibrated with outer tank concrete. Conditions C and D involve mixtures of groundwater with Reduced Region II pore fluid and Oxidized Region II pore fluid. The fraction of pore fluid from the tank grout was determined by calculating mixing curves of the two end-member water compositions (Figure 4). Pore fluid compositions for Conditions C and D were chosen to be as different as possible from either end member. This turns out to be a fractional mixture of approximately 0.1 tank grout pore fluid and 0.9 groundwater. The compositions of the pore fluids associated with the four submerged tank conditions are shown in Table 3. These are treated here as independent cases rather than as conditions linked by the progression of grout degradation. Conditions C and D could be linked as Reduced Region II pore water would evolve into Oxidized Region II pore water. Condition D would then degrade into Oxidized Region III of Table 2. However, for the submerged tanks the

transition times for the progression through each condition are different than for the non-submerged tanks. This is because groundwater is the fluid driving tank grout degradation rather than infiltration. The transition times are presented in a later section and their derivation discussed in Appendix B.

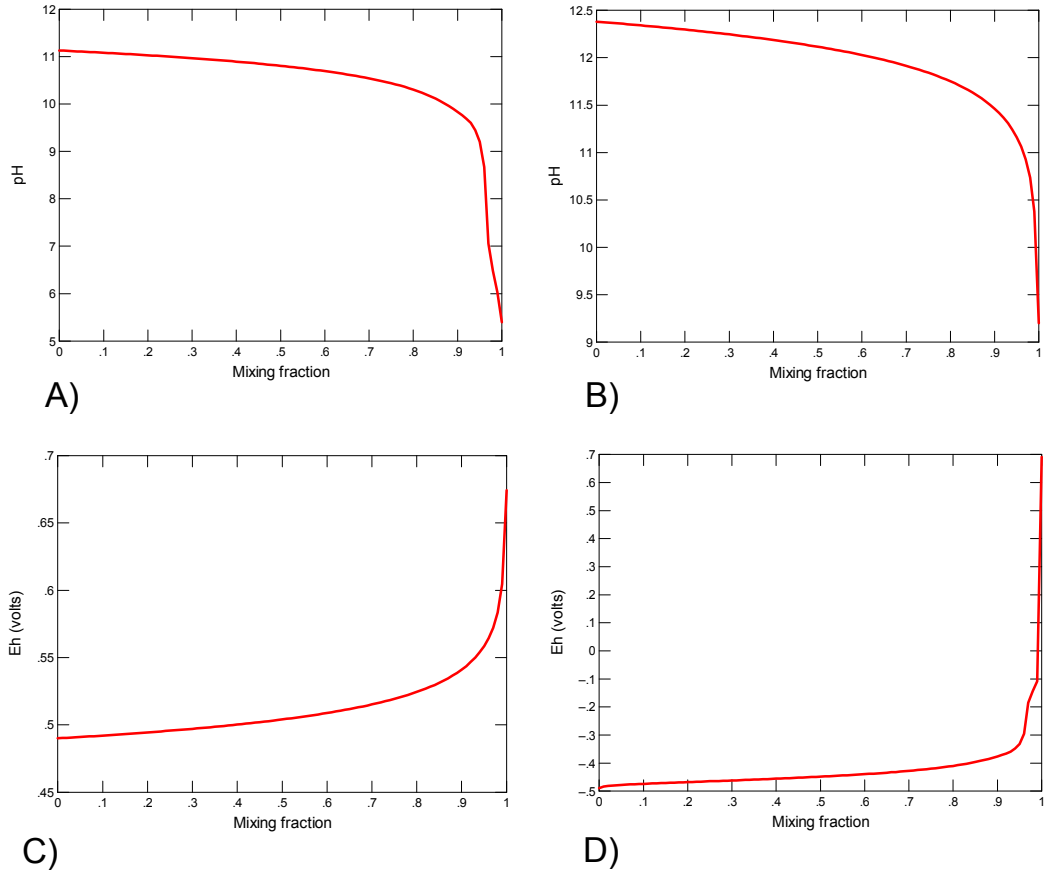


**Figure 4: Mixing curves of groundwater and tank grout pore fluid (x-axis is fraction of groundwater in mixture); A) pH of groundwater + reduced Region II, B) pH of groundwater + oxidized Region II, C) Eh of groundwater + reducing Region II, and D) Eh of groundwater + oxidizing Region II.**

**Table 3: Calculated porewater compositions for the various conditions in the CZ of partially submerged tanks.**

| | Porewater Conditions | | | |
|---|---|---|---|---|
| **Parameter** | **A** | **B** | **C** | **D** |
| pH | 5.4 | 9.30 | 9.83 | 9.84 |
| Eh (volts) | 0.369 | 0.266 | -0.380 | 0.620 |
| Ca (moles/liter) | $6.2 \times 10^{-5}$ | $2.0 \times 10^{-4}$ | $2.1 \times 10^{-4}$ | $2.1 \times 10^{-4}$ |
| Na | $4.4 \times 10^{-5}$ | $4.3 \times 10^{-5}$ | $4.0 \times 10^{-5}$ | $4.1 \times 10^{-5}$ |
| Cl | $8.5 \times 10^{-5}$ | $1.5 \times 10^{-4}$ | $2.7 \times 10^{-4}$ | $2.6 \times 10^{-4}$ |
| $HCO_3^-$ | $9.8 \times 10^{-5}$ | $2.4 \times 10^{-4}$ | $4.2 \times 10^{-5}$ | $4.2 \times 10^{-5}$ |
| $SO_4^{-2}$ | $6.3 \times 10^{-6}$ | $6.2 \times 10^{-6}$ | $5.4 \times 10^{-6}$ | $6.5 \times 10^{-6}$ |

Condition A: Porewater = Groundwater
Condition B: Porewater = Groundwater equilibrated with calcite
Condition C: Porewater = Mixture 0.9 Groundwater + 0.1 Reduced Region II Porewater
Condition D: Porewater = Mixture 0.9 Groundwater + 0.1 Oxidized Region II Porewater

## *Selecting Solubility Controlling Phases*

A fundamental part of establishing solubility controlled waste release rates is selection of a solubility controlling phase for each radionuclide. For some of the radionuclides of interest there are studies in the literature that can guide selection of solubility controls, for others it is a professional judgment. For this reason, selection of solubility controlling phases was generally very conservative, meaning that where multiple phases of a radionuclide were possible, the one with the highest solubility was selected. This analysis is part of a performance assessment that adopts a risk-based approach. If conservative assumptions about solubility result in an unacceptable estimated risk, additional constraints on solubility can be considered such as alternate phases or co-precipitation.

There are two factors that determine the solubility of a phase – the composition and the structure. For phases with the same composition, amorphous forms usually have higher solubilities than crystalline forms. Thus, where thermodynamic data existed, the amorphous forms were selected for solubility controls. For most, hydroxides were chosen over oxides because the hydroxide of an element usually has a higher solubility than the oxide. For many radionuclides, carbonate phases were selected. This was particularly true for the Bradbury and Sarott Region III states because of the higher partial pressures of $CO_2$. Carbonate phases normally precipitate easily from solution (example, Noyes, 1994) and their occurrence in the grouted tanks was considered to be plausible.

Two special cases of mineral selection are becquerelite [$Ca(UO_2)_6O_4(OH)_6 \cdot 8H_2O$] for uranium and $Tc_2S_7$ for technetium. These phases were selected because they have been identified elsewhere in samples subject to conditions similar to those expected for the closed tanks. Becquerelite is stable at cementitious conditions and has been identified in experiments at these conditions by Atkins et al. (1988) and Moroni and Glasser (1995). Likewise, Lukens et al.(2004) identified $Tc_2S_7$ in SRS reducing grout experiments at conditions near those expected for closed tanks.

The professional judgment used in selecting solubility controlling phases followed the general flow of Figure 5. For each radionuclide the process began with an examination of the literature for occurrence of a stable phase with reliable thermodynamic data at conditions prevalent in the tanks or cementitious systems. If one was found, it was selected. Examples are becquerelite for uranium and $Tc_2S_7$ for technetium in reduced grout. If none was found, a list of other phases that contain components found in the tanks and having reliable thermodynamic data was assembled. The stability fields of these phases were examined and phases stable at conditions corresponding to those of the conceptual model were retained. If there were appropriate geologic or industrial process analogues cited in the literature they were selected. Examples are radium sulfate and strontium carbonate. If there were no analogues cited in the literature, but the hydroxide was stable, it was retained. If reliable thermodynamic data was available for the amorphous hydroxide then it was selected. If not, the crystalline hydroxide was selected. If hydroxide was not stable, an appropriate non-hydroxide with the highest solubility was selected. An example is $AmOHCO_3$. The process attempted to balance scientific knowledge with the need to be cautious and biased toward higher solubilities.

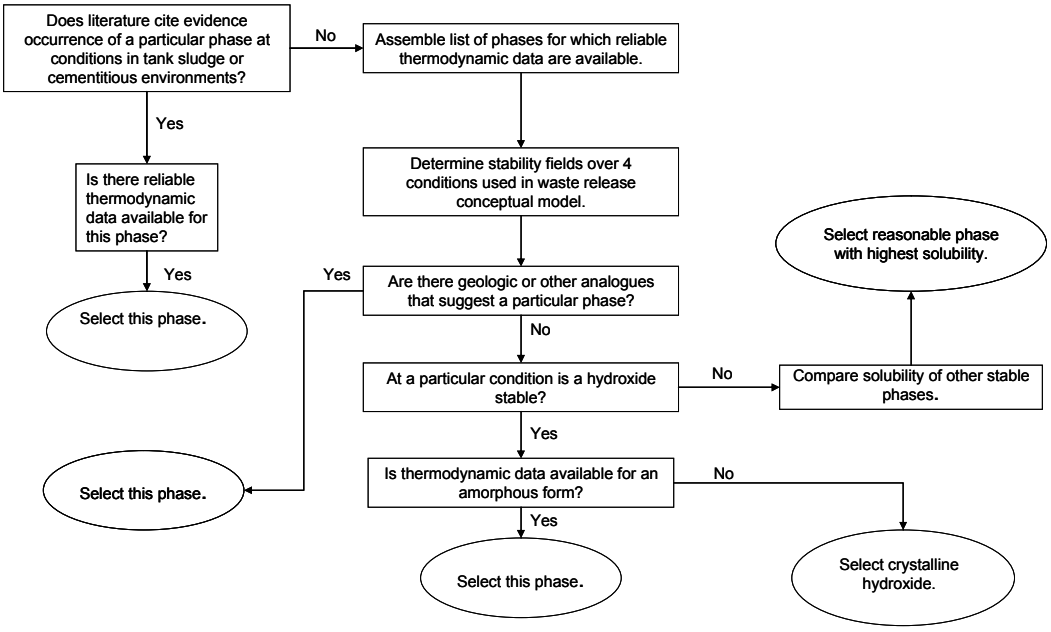


**Figure 5: General flow in the use of professional judgment to select solubility controlling phases.**

## *Adsorption Controls*

In the implementation of the conceptual model for waste release it was evident that adsorption controls would play a minor role (Appendix A). For this reason and the inability to calculate reliable adsorption parameters for most of the radionuclides of interest, it was decided to use only solubility controls to account for waste release in fate and transport models. This avoids the needs to make assumptions about the mineralogy of the residual waste layer, the abundance of minerals, and their surface areas based on very limited information.

It is thought that the importance of solubility controls is minimal because for most of the radionuclides the mass of matrix minerals in the residual waste will be too low to adsorb a substantial fraction of the radionuclide inventory (see Appendix A). In other words, the inventories of most radionuclides exceed the adsorption capacity of the residual waste. The fact that the radionuclides present in the residual waste remain after extensive washing supports the assumption that they occur in a form less labile than adsorbed.

In an equilibrium model, the assumption that solubility rather than adsorption controls waste release is conservative, resulting in faster overall release of radionuclides. This is because the maximum concentration that can desorb is controlled by solubility. In effect, if the partitioning coefficient (Kd) is low enough that a concentration is released that exceeds solubility, some of the radionuclide will precipitate bringing the concentration down to solubility. The waste release rate will drop below that dictated by solubility when the radionuclide inventory is depleted to where the concentration released is below solubility. At higher Kd values the concentration released at any given time will always be below the concentration dictated by solubility. Thus, time until complete release of a radionuclide using adsorption controls will always be longer than when only solubility controls are used. This is demonstrated in Figure 6, an example of uranium release from the CZ under reducing conditions, if there was a total inventory of 10 moles and a solubility of $3.5 \times 10^{-5}$ moles/liter. Adsorption controls result in an overall slower release of uranium.

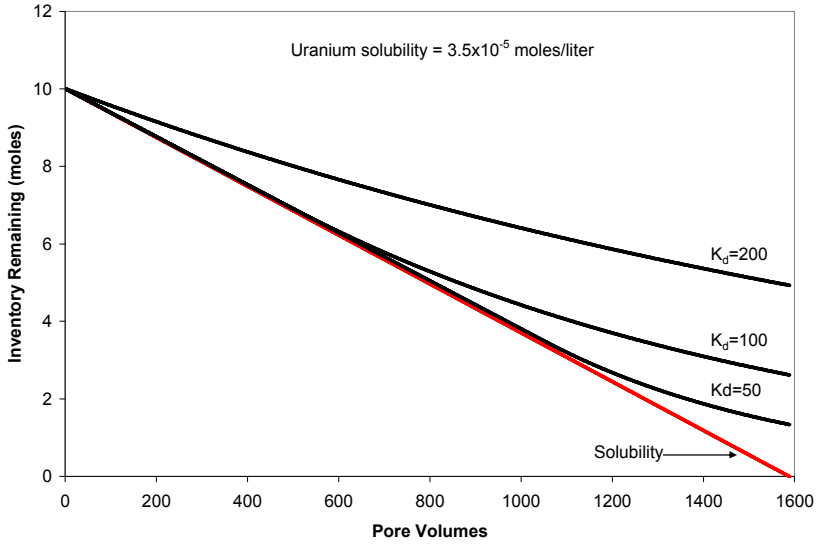


**Figure 6: Comparison of solubility only and adsorption only (Kd values in ml/g) controls on uranium release assuming a total inventory of 10 moles and a solubility of $3.5 \times 10^{-5}$ moles/liter.**

**Solubility Values**

Table 4 shows solubility values and controlling phases for all of the elements of interest at each of the chemical states of interest. These apply to all F-Area tanks and the non-submerged tanks in H-Area. Solubilities of four of the radionuclides were not calculated because of lack of thermodynamic data (Bk-249, Cf-249, Rh-106, and Te-125m). However, each of these has either a very small inventory or a short half-life and is unlikely to be an issue at exposure points. Several of the elements have no identified solubility controls and it is recommended that their release be modeled as instantaneous (within the first pore volume). For Tc and Se, concentrations in a Tank 18 dip sample were much lower than expected for identifiable solubility controls. This suggests that there may be phases present that are not well known or that they may be co-precipitated with another phase.

**Table 4: Calculated solubilities of radionuclides in each of the chemical states shown in Table 1.**

| | Oxidized Region II | | Oxidized Region III | |
|---|---|---|---|---|
| | **Controlling Phase** | **Solubility (moles/liter)** | **Controlling Phase** | **Solubility (moles/liter)** |
| **Ac** | La(OH)3 | 4.0E-5 | La2(CO3)3:8H2O | 1.6E-08 |
| **Am** | Am(OH)3 (am) | 8.6E-9 | AmOHCO3 | 4.9E-08 |
| **Ba** | Witherite(BaCO3) | 6.4E-7 | Witherite(BaCO3) | 8.7E-09 |
| **Bk** | short half-life | | short half-life | |
| **C** | Calcite | 9.6E-6 | Calcite | 5.8E-4 |
| **Ce** | Ce(OH)3 | 1.2E-5 | Ce(OH)3 | 3.4E-04 |
| **Cf** | small inventory | | small inventory | |
| **Cm** | Cm(OH)3 | 5.1E-10 | CmOHCO3 | 4.2E-7 |
| **Co** | CoFe2O4 | 5.0E-10 | CoFe2O4 | 5.9E-13 |
| **Cs** | No solubility control | | No solubility control | |
| **Eu** | Eu(OH)3 | 1.2E-8 | EuOHCO3 | 1.2E-06 |
| **I** | No solubility control | | No solubility control | |
| **Nb** | No solubility control | | No solubility control | |
| **Ni** | NiFe2O4 | 1.2E-10 | NiFe2O4 | 1.2E-07 |
| **Np** | NpO2OH(am) | 6.8E-7 | Np(OH)4 | 1.3E-4 |
| **Pa** | No solubility control | | No solubility control | |
| **Pm** | Pm(OH)3(am) | 1.3E-8 | Pm2(CO3)3 | 1.8E-07 |
| **Pr** | Pr(OH)3 | 7.9E-6 | Pr(OH)3 | 9.7E-08 |
| **Pu** | Pu(OH)4 | 3.0E-7 | Pu(OH)4 | 5.7E-05 |
| **Ra** | RaSO4 | 9.1E-6 | RaSO4 | 3.8E-06 |
| **Rh** | short half-life | | short half-life | |
| **Ru** | RuO2.2H2O(am) | 1.5E-3 | RuO2.2H2O(am) | 7.6E-07 |
| **Sb** | Sb(OH)3 | 9.5E-8 | Sb(OH)3 | 8.0E-08 |
| **Se** | No solubility control | | No solubility control | |
| **Sm** | Sm(OH)3(am) | 5.6E-6 | Sm(OH)3(am) | 4.4E-06 |
| **Sn** | Cassiterite (SnO2) | 2.7E-8 | Cassiterite (SnO2) | 2.7E-08 |
| **Sr** | Strontianite (SrCO3) | 2.2E-5 | Strontianite (SrCO3) | 4.1E-06 |
| **Tc** | No solubility control | | No solubility control | |
| **Te** | short half-life | | short half-life | |
| **Th** | Th(OH)4 | 4.2E-7 | Th(OH)4 | 4.2E-07 |
| **U** | Becquerelite | 3.4E-7 | Becquerelite | 3.4E-05 |
| **Y** | Y(OH)3 | 1.9E-8 | Y(OH)3 | 5.1E-05 |

**Table 4 (cont.): Calculated solubilities of radionuclides of interest.**

| | Reduced Region II | | Reduced Region III | |
|---|---|---|---|---|
| | **Controlling Phase** | **Solubility (moles/liter)** | **Controlling Phase** | **Solubility (moles/liter)** |
| **Ac** | La(OH)3 | 4.0E-5 | La2(CO3)3:8H2O | 1.4E-08 |
| **Am** | Am(OH)3 | 8.8E-9 | AmOHCO3 | 7.7E-08 |
| **Ba** | Witherite(BaCO3) | 6.5E-7 | Witherite(BaCO3) | 5.6E-09 |
| **Bk** | short half-life | | short half-life | |
| **C** | Calcite | 9.6E-6 | No solubility control | |
| **Ce** | Ce(OH)3 | 1.1E-5 | Ce(OH)3 | 4.5E-05 |
| **Cf** | small inventory | | small inventory | |
| **Cm** | Cm(OH)3 | 5.2E-10 | CmOHCO3 | 5.1E-08 |
| **Co** | CoFe2O4 | 4.8E-10 | CoFe2O4 | 5.4E-13 |
| **Cs** | No solubility control | | No solubility control | |
| **Eu** | Eu(OH)3 | 1.2E-8 | EuOHCO3 | 1.2E-06 |
| **I** | No solubility control | | No solubility control | |
| **Nb** | No solubility control | | No solubility control | |
| **Ni** | Heazlewoodite (Ni3S2) | 4.3E-11 | Polydimite (Ni3S4) | 1.2E-10 |
| **Np** | Np(OH)4 | 4.8E-9 | Np(OH)4 | 1.6E-09 |
| **Pa** | No solubility control | | No solubility control | |
| **Pm** | Pm(OH)3(am) | 1.3E-8 | Pm2(CO3)3 | 1.8E-07 |
| **Pr** | Pr(OH)3(am) | 7.8E-6 | Pr2(CO3)3 | 9.5E-08 |
| **Pu** | Pu(OH)4 | 1.7E-9 | Pu(OH)4 | 2.9E-09 |
| **Ra** | RaSO4 | 6.0E-6 | RaSO4 | 4.6E-04 |
| **Rh** | short half-life | | short half-life | |
| **Ru** | RuS2 | 3.3E-50 | RuS2 | 9.0E-11 |
| **Sb** | Sb(OH)3 | 9.4E-8 | Sb(OH)3 | 8.0E-08 |
| **Se** | Ferroselite (FeSe2) | 8.7E-6 | Ferroselite (FeSe2) | 2.4E-02 |
| **Sm** | Sm(OH)3(am) | 5.5E-6 | Sm(OH)3(am) | 2.6E-04 |
| **Sn** | Cassiterite (SnO2) | 2.7E-8 | Cassiterite (SnO2) | 2.7E-08 |
| **Sr** | Strontianite (SrCO3) | 2.3E-5 | Strontianite (SrCO3) | 2.7E-06 |
| **Tc** | Tc2S7 | 1.2E-32 | Tc2S7 | 2.8E-38 |
| **Te** | short half-life | | short half-life | |
| **Th** | Th(OH)4 | 4.2E-7 | Th(OH)4 | 4.2E-07 |
| **U** | UO2(am) | 3.5E-5 | UO2(am) | 3.5E-05 |
| **Y** | Y(OH)3 | 1.8E-8 | Y(OH)3 | 1.8E-04 |

**Solubilities for H-Area Partially Submerged Tanks**

The solubilities of discrete phases of radionuclides in partially submerged tanks in H-Area were calculated using pore fluid composition for the four conditions shown in Table 3. These are shown with the assumed solubility controlling phases in Table 5.

**Table 5: Calculated solubilites for radionuclides in pore waters of the four conditions listed in Table 2.**

| | Submerged Condition A | | Submerged Condition B | |
|---|---|---|---|---|
| | CZ Submerged – Porewater = Groundwater | | CZ Submerged – Porewater = Groundwater + Calcite | |
| | Controlling Phase | Solubility (moles/liter) | Controlling Phase | Solubility (moles/liter) |
| **Ac** | $La_2(CO_3)_3 \cdot 8H_2O$ | 3.1E-5 | $La_2(CO_3)_3:8H_2O$ | 1.4E-8 |
| **Am** | $AmOHCO_3$ | 1.1E-4 | $Am(OH)_3$(am) | 6.0E-8 |
| **Ba** | Witherite($BaCO_3$) | 2.0E-5 | Witherite($BaCO_3$) | 3.9E-4 |
| **Bk** | short half-life | | short half-life | |
| **C** | No solubility control | | no solubility control | |
| **Ce** | $Ce_2(CO_3)_3 \cdot 8H_2O$ | 3.8E-5 | $Ce_2(CO_3)_3 \cdot 8H_2O$ | 6.4E-8 |
| **Cf** | small inventory | | small inventory | |
| **Cm** | $Cm(OH)_3$ | 7.4E-4 | $CmOHCO_3$ | 6.3E-9 |
| **Co** | $CoFe_2O_4$ | 9.9E-11 | $CoFe_2O_4$ | 6.8E-12 |
| **Cs** | No solubility control | | No solubility control | |
| **Eu** | $Eu_2(CO_3)_3 \cdot 8H_2O$ | 1.3E-5 | $Eu(OH)_3$ | 1.5E-6 |
| **I** | No solubility control | | No solubility control | |
| **Nb** | No solubility control | | No solubility control | |
| **Ni** | No solubility control | | $NiFe_2O_4$ | 1.4E-9 |
| **Np** | Np(OH)4 | 1.4E-4 | Np(OH)4 | 1.1E-5 |
| **Pa** | No solubility control | | No solubility control | |
| **Pm** | $Pm2(CO_3)_3$ | 5.6E-5 | $Pm2(CO_3)_3$ | 1.9E-7 |
| **Pr** | $Pr2(CO_3)_3$ | 4.7E-5 | $Pr2(CO_3)_3$ | 1.0E-7 |
| **Pu** | $Pu(OH)_4$ | 2.0E-9 | $Pu(OH)_4$ | 1.7E-9 |
| **Ra** | $RaSO_4$ | 6.7E-6 | $RaSO_4$ | 7.4E-6 |
| **Rh** | short half-life | | short half-life | |
| **Ru** | $Ru(OH)_3 \cdot H_2O$(am) | 7.6E-8 | $RuO_2 \cdot 2H_2O$(am) | 7.1E-7 |
| **Sb** | $Sb(OH)_3$ | 8.0E-8 | $Sb(OH)_3$ | 8.1E-8 |
| **Se** | No solubility control | | No solubility control | |
| **Sm** | $Sm_2(CO_3)_3$ | 6.0E-5 | $Sm(OH)_3$(am) | 2.0E-6 |
| **Sn** | cassiterite ($SnO_2$) | 2.7E-8 | cassiterite ($SnO_2$) | 2.7E-8 |
| **Sr** | strontianite ($SrCO_3$) | 1.0E-3 | strontianite ($SrCO_3$) | 1.4E-6 |
| **Tc** | No solubility control | | No solubility control | |
| **Te** | short half-life | | short half-life | |
| **Th** | $Th(OH)_4$ | 4.5E-7 | $Th(OH)_4$ | 4.2E-7 |
| **U** | Schoepite | 5.8E-6 | Becquerelite | 2.4E-6 |
| **Y** | No Solubility control | | $Y(OH)_3$ | 3.8E-7 |

**Table 5: (Continued)**

| | Submerged Condition C | | Submerged Condition D | |
|---|---|---|---|---|
| | CZ Submerged – Porewater = Mixture 0.9 Groundwater + 0.1 Reduced Region II Porewater | | CZ Submerged – Porewater = Mixture 0.9 Groundwater + 0.1 Oxidized Region II Porewater | |
| | Controlling Phase | Solubility (moles/liter) | Controlling Phase | Solubility (moles/liter) |
| **Ac** | $La_2(CO_3)_3 \cdot 8H_2O$ | 2.2E-8 | $La_2(CO_3)_3$:$8H_2O$ | 2.3E-8 |
| **Am** | $Am(OH)_3$(am) | 1.3E-7 | $Am(OH)_3$(am) | 1.2E-7 |
| **Ba** | Witherite($BaCO_3$) | 6.2E-9 | Witherite($BaCO_3$) | 6.1E-9 |
| **Bk** | short half-life | | short half-life | |
| **C** | Calcite ($CaCO_3$) | 5.2E-4 | Calcite ($CaCO_3$) | 2.1E-4 |
| **Ce** | $Ce_2(CO_3)_3 \cdot 8H_2O$ | 5.1E-7 | $Ce_2(CO_3)_3 \cdot 8H_2O$ | 5.9E-7 |
| **Cf** | tiny inventory | | tiny inventory | |
| **Cm** | $Cm(OH)_3$ | 1.1E-8 | Cm(OH)3 | 1.0E-8 |
| **Co** | $CoFe_2O_4$ | 2.3E-11 | $CoFe_2O_4$ | 2.4E-11 |
| **Cs** | No solubility control | | No solubility control | |
| **Eu** | $Eu(OH)_3$ | 1.2E-7 | $Eu(OH)_3$ | 1.2E-7 |
| **I** | No solubility control | | No solubility control | |
| **Nb** | No solubility control | | No solubility control | |
| **Ni** | $NiFe_2O_4$ | 1.7E-10 | $NiFe_2O_4$ | 1.6E-10 |
| **Np** | $Np(OH)_4$ | 1.6E-9 | $NpO_2OH_{(am)}$ | 2.5E-5 |
| **Pa** | No solubility control | | No solubility control | |
| **Pm** | $Pm(OH)_3$(am) | 2.3E-8 | $Pm(OH)_3$(am) | 1.3E-8 |
| **Pr** | $Pr_2(CO_3)_3$ | 2.7E-7 | $Pr_2(CO_3)_3$ | 2.8E-7 |
| **Pu** | $Pu(OH)_4$ | 1.7E-9 | $PuO_2(OH)_2$ | 4.5E-10 |
| **Ra** | $RaSO_4$ | 7.5E-6 | $RaSO_4$ | 7.2E-6 |
| **Rh** | short half-life | | short half-life | |
| **Ru** | $RuS_2$ | 4.6E-48 | $RuO_2 \cdot 2H_2O$(am) | 1.2E-6 |
| **Sb** | $Sb(OH)_3$ | 8.1E-8 | $Sb_2O_5$ | 7.5E-22 |
| **Se** | No solubility control | | No solubility control | |
| **Sm** | $Sm(OH)_3$(am) | 3.4E-7 | $Sm(OH)_3$(am) | 3.4E-7 |
| **Sn** | cassiterite ($SnO_2$) | 2.7E-8 | cassiterite ($SnO_2$) | 2.7E-8 |
| **Sr** | strontianite ($SrCO_3$) | 3.0E-6 | strontianite ($SrCO_3$) | 2.9E-6 |
| **Tc** | $Tc_2S_7$ | 1.1E-31 | No solubility control | |
| **Te** | short half-life | | short half-life | |
| **Th** | $Th(OH)_4$ | 4.2E-7 | $Th(OH)_4$ | 4.2E-7 |
| **U** | $UO_2$(am) | 3.5E-5 | Becquerelite | 2.5E-7 |
| **Y** | $Y(OH)_3$ | 8.5E-9 | $Y(OH)_3$ | 8.4E-9 |

## *Uncertainties in Solubility Calculations*

There are uncertainties in the calculation of the solubilities presented here. Much of the uncertainty is because of unknowns related to the CZ and how the conditions it will experience will evolve with time. Some is due to the limited amount of thermodynamic data available for many of the radionuclides of interest. The uncertainty can be reduced by laboratory studies, but significant uncertainty will always remain. For example, with very careful and detailed analyses, the actual form the dominant radionculides take in the CZ might be determined. Nevertheless, there would still be considerable uncertainty because as conditions change from initial tank grouting to several thousand years in the future, these radionuclide forms are likely to change as well. The best way to manage this uncertainty in implementation of this conceptual model is to be as conservative in assumptions as is reasonable.

## Choice of Controlling Phase

For many radionuclides the choice of the solubility controlling phase is the largest uncertainty in calculated solubility values. In this analysis the choice of controlling phase was biased toward higher solubility phases by not considering many phases with low solubilities. For example, where there was thermodynamic data available for both amorphous and crystalline phases of the same stoichiometry, the amorphous phase was chosen because amorphous phases generally have higher solubilities than their crystalline counterparts. Thus, the solubilities reported here may be biased high by many orders of magnitude for many elements. A good example is uranium. Table 6 compares uranium solubilities calculated for Conditions 2 and 3 (Oxidized Region II and Reduced Region II) with solubilities calculated for other potential solubility controlling phases. Choice of becquerelite yields a calculated controlling solubility that is 7 orders of magnitude higher than if $CaUO_4$ was chosen. Yet, becquerelite was chosen here because it is common in cementitious systems. Choice of the amorphous form of $UO_2$ rather than the crystalline form (uraninite) yields a solubility that is 5 orders of magnitude higher. To further complicate the issue, there is ample evidence to suggest that uranium concentrations may also be limited by silicate and phosphate phases (Wellman et al., 2007; Moroni and Glasser, 1995) that were not considered in this evaluation.

**Table 6: Comparison of calculated solubilities of various uranium phases.**

| **Phase Chosen for Oxidizing Region II** | **Solubility** (mole/liter) |
|---|---|
| Becquerelite | $3.4 \times 10^{-7}$ |
| **Other Potential Solubility Controlling Phases for Oxidizing Region II** | |
| $CaUO_4$ | $1.8 \times 10^{-14}$ |
| Schoepite | $1.8 \times 10^{-5}$ |
| **Phase Chosen for Reducing Region II** | |
| $UO_2$ (amorphous) | $3.5 \times 10^{-5}$ |
| **Other Potential Solubility Controlling Phases for Reducing Region II** | |
| Uraninite (crystalline $UO_2$) | $3.9 \times 10^{-10}$ |

Another example of the importance of controlling phase selection is neptunium. $Np(OH)_4$ and $NPO_{2(am)}$ have calculated solubilities of approximately $5x10^{-9}$ moles/liter under Reducing Region II conditions, whereas the calculated solubility of crystalline $NpO_2$ is $2.6x10^{-20}$ moles/liter. Yet, Lilley et al. (2009) measured a solubility of approximately $10^{-13}$ moles/liter in reducing cementitious material, but the controlling phase was unknown.

The main reason for choosing high solubility phases over low solubility phases is that precipitation of higher solubility phases are often kinetically favored over low solubility phases. If they weren't, the low solubility phases would always be the controlling phases. Choosing higher solubility phases eliminates consideration of kinetic arguments for why a lower solubility phases would be expected.

For some elements, phases other than the amorphous hydroxides were chosen. For nickel and cobalt, phases with the stoichiometry of $XFe_2O_4$ were chosen because there is a possibility that precipitation of these phases would be catalyzed at the surface of hematite or other ferric iron phases present. For other elements, sulfate or carbonate phases were chosen because these are known to precipitate readily as pipe or tank scale and thus it was assumed that kinetics would not inhibit their precipitation in the tanks. For tin, the database for appropriate solid phases is so small that cassiterite ($SnO_2$) was considered to be the most likely phase to precipitate of those for which there is data.

One way to manage uncertainty related to choice of solubility controlling phase is to consider the probability of different phases occurring. For example, $Pu(OH)_4$ was selected here as the solubility controlling phase. Yet, the more thermodynamically stable $PuO_2$ is feasible, particularly at the elevated temperatures (~80$^{o}$C; Caldwell, 1997) that will occur from initial grout hydration. If $PuO_2$ was the controlling phase, it would have a large effect on waste release because its calculated solubility under Reducing Region II conditions is $1.3x10^{-17}$ moles/liter compared to the $Pu(OH)_4$ solubility of $1.7x10^{-9}$ moles/liter. Table 7 shows a possible distribution of phases for plutonium, uranium, neptunium, and technetium, where the distributions are weighted to account for the possibility of different phases. The distributions chosen here are not rigorously or mathematically determined. They are based on professional judgment that accounts for observations in the literature, thermodynamic stability, etc.

**Table 7: Possible estimated distributions of various phases controlling solubility of plutonium, neptunium, technetium, and uranium.**

| Oxidized Region II | | | |
|---|---|---|---|
| | **Controlling Phase** | **Solubility (moles/liter)** | **Estimated Distribution** |
| **Plutonium** | $Pu(OH)_4$ | 3.0E-07 | 0.7 |
| | $PuO_2$ | 2.3E-15 | 0.2 |
| | $PuO_2(OH)_2$ | 1.9E-11 | 0.1 |
| | | | |
| **Neptunium** | $NpO_2(OH)(am)$ | 6.8E-07 | 0.7 |
| | $Np_2O_5$ | 9.6E-10 | 0.2 |
| | $NpO_2$ | 1.2E-10 | 0.1 |
| | | | |
| **Technetium** | No Solubility Control | | |
| | | | |
| **Uranium** | Becquerelite | 3.4E-07 | 0.5 |
| | $CaUO_4$ | 1.8E-14 | 0.3 |
| | Schoepite | 1.8E-5 | 0.2 |
| **Reduced Region II** | | | |
| **Plutonium** | $Pu(OH)_4$ | 1.7E-09 | 0.7 |
| | $PuO_2$ | 1.3E-17 | 0.3 |
| | | | |
| **Neptunium** | $Np(OH)_4$ | 4.8E-09 | 0.7 |
| | NpO(am) | 5.1E-9 | 0.2 |
| | $NpO_2$ | 2.6E-20 | 0.1 |
| | | | |
| **Technetium** | $Tc_2S_7$ | 1.2E-32 | 0.8 |
| | $TcO_2.2H_2O$ | 3.3E-08 | 0.2 |
| | | | |
| **Uranium** | UO2(am) | 3.5E-05 | 0.7 |
| | Uraninite | 3.9E-10 | 0.3 |

## Uncertainty in Thermodynamic Data

Uncertainty in thermodynamic data can result in large discrepancies in mineral solubility. The thermodynamic database used for the solubility calculations in Table 4 was the "thermo.com.V8.R6+" an update of earlier compilations by Lawrence Livermore National Laboratory and provided with The Geochemist's Workbench® (Bethke, 2005). For any given solubility calculation there are numerous thermodynamic quantities involved, each of which has an uncertainty. The uncertainties in each of these compound and can lead to solubility calculations that have a range of uncertainty that spans several orders of magnitude. Typically, the least studied constituents have the highest uncertainty in their thermodynamics, but even well studied constituents can have high thermodynamic uncertainties if their chemistries are

complicated. For example, uranium is well studied but has multiple oxidations states, can form aqueous complexes with a variety of anions and cations, and can form dozens of solid phases. Accounting for all of these complexities in experiments measuring thermodynamic quantities is extremely difficult, often resulting in very different values reported for the same quantity. The solubility of the uranium mineral becquerelite is an example. Table 8 shows values for log K measured in four studies for the dissolution reaction:

$$Ca(UO_2)_6O_4(OH)_6{\cdot}8H_2O_{(s)} + 14H^+ = 6UO_2^{+2} + Ca^{+2} + 18H_2O$$

**Table 8: Values of log K for reaction above from various studies.**

| log K | Reference |
|---|---|
| 41.89 | Vochten and Van Haverbeke (1990) |
| 43.6 | Sandino and Grambow (1994) |
| 29 | Casas et al. (1997) |
| 41.4 | Rai et al. (2002) |

The solubility calculated for becquerelite using these values varies by 2 orders of magnitude for the chemical composition associated with Condition 1. The reason the calculated solubility only varies by 2 orders of magnitude despite the 14.6 orders of magnitude variation in the equilibrium constant is that, at these conditions, other thermodynamic quantities exert greater control on the solubility of becquerelite. At pH=12.3 and oxidizing conditions, the primary control on the solubility is the association constant of the dominant aqueous uranium complex, $UO_2(OH)_4^{-2}$.

Figure 7 shows the results of a simple analysis of the sensitivity of calculated solubilities to the equilibrium constant of the dissolution reaction and the association constant of the dominant aqueous species of three pertinent radionuclides. The solubilities of uranium, plutonium, and neptunium were calculated using the controlling solid phases of becquerelite, $Pu(OH)_4$, and $NpO_2(OH)_{am}$. This was done for four different scenarios in which the solubility constant of the solid and the association constant of the dominant aqueous complex were varied in different ways. In scenario A, the equilibrium constant of the dissolution reaction was varied ±1 order of magnitude from that used in the original calculation and all other constants were the same as used in the original calculation. In scenario B, the association constant for the dominant aqueous species was varied by ±1 order of magnitude while all other constants remained the same as in the original calculation. In scenario C, the association constant of the dominant species and the equilibrium constant for the dissolution reaction were varied in the same direction ± 1 order of magnitude. In scenario D, the two constants were varied in opposite directions ±1 order of magnitude.

The results show that the maximum variation in solubility is when the two constants are varied in the opposite directions, scenario D. The results also show the insensitivity of the calculated solubility to the equilibrium constant of the dissolution reaction relative to the association constant of the dominant species when the dominant aqueous species is not the same as the aqueous species used in the dissolution reaction. As chemical conditions approach the stability of the dominant aqueous species in the dissolution reaction the calculated solubility will become more sensitive to the equilibrium constant of this reaction.

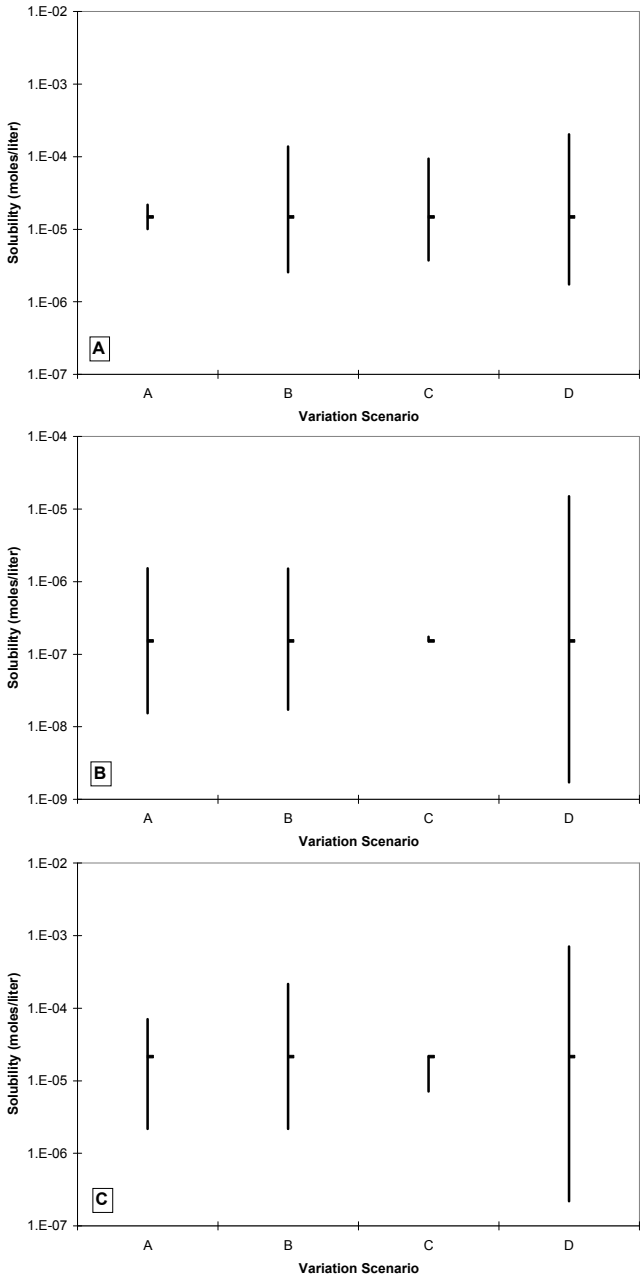


**Figure 7: Effect of varying different thermodynamic parameters on solubility of A) becquerelite, B) Pu(OH)4, and C) NpO2(OH)(am). Vertical lines show variation in solubility in each scenario, horizontal tick marks show the solubility reported in this study. See the text for explanation of the scenarios.**

The Nuclear Energy Agency's Organisation for Economic Co-Operation and Development (OECD) is developing a thermodynamic database for species and reactions pertinent to the nuclear industry and has published volumes specific to several radioactive elements. Table 9 shows the range in uncertainty reported in this database for association constants of aqueous species of several radioactive elements.

**Table 9: Variation in association constants of aqueous species of various elements of interest.**

| Element | Range of Uncertainty in log K | Reference |
|---|---|---|
| U | ±0.02 to ±2.00 | Grenthe et al., 1992 |
| Pu | ±0.09 to ±3.00 | Lemire et al., 2001 |
| Np | ±0.06 to ±2.69 | Lemire et al., 2001 |
| Tc | ±0.15 to ±1.7 | Rard et al., 1999 |

From the sensitivity analysis shown in Figure 7 and Table 9 we assume a maximum uncertainty in calculated solubilities due to thermodynamic uncertainty to be 2 orders of magnitude for all elements. In general, it will be smaller for well studied elements and larger for those that are rarely studied. This assumption is not a rigorous analysis of uncertainty, but even if the uncertainty due to thermodynamic data is an order of magnitude higher, it is unlikely to outweigh the uncertainty in choice of solubility controlling phase.

## Co-precipitation

Co-precipitation as defined here is the incorporation of an element into the crystal structure of a solid phase that is predominantly made of other elements or the trapping of an element within the bulk mass of a phase made up of other elements, but not necessarily within the crystal lattice. The incorporated element is often referred to as a trace or minor element in the solid phase. This differs from adsorption where an element is bound to the surface layers of a solid phase and is available for equilibration with pore fluids. The bulk of a co-precipitated trace element is not available for interaction with pore fluids until the parent phase is dissolved.

An example of co-precipitation that can be treated thermodynamically is $Cr^{+3}$ incorporated into the structure of $Fe(OH)_3$. This can be considered thermodynamically in a simple way by the reaction:

$$Cr^{+3} + Fe(OH)_3 = Cr(OH)_3 + Fe^{+3}$$

With an equilibrium constant of:

$$K = \frac{aFe^{+3} \times ACr(OH)_3}{aCr^{+3} \times AFe(OH)_3}$$

where $aFe^{+3}$ and $aCr^{+3}$ are the activities of the aqueous species and $ACr(OH)_3$ and $AFe(OH)_3$ are the activities of these components in the precipitated solid. The equilibrium relationship can be rearranged to:

$$K \times \frac{AFe(OH)_3}{ACr(OH)_3} = \frac{aFe^{+3}}{aCr^{+3}}$$

Thus, the amount of chromium that precipitates with $Fe(OH)_3$ is related to the ratio of $Fe^{+3}$ to $Cr^{+3}$ in the aqueous solution by the equilibrium constant, sometimes referred to as the distribution coefficient (D).

Co-precipitation in which the element of interest is not part of the crystal structure of the main phase cannot be treated thermodynamically. Yet, when the molar ratio in solution of an element of interest to a "carrier" element is very small, co-precipitation with the carrier phase can remove much of the element of interest from the solution providing that the element of interest has not already precipitated and settled out of solution. Table 10 presents the molar ratios of Pu-239, U-238, and Tc-99 to iron in Tanks 19 and 20 residual waste. Barney and Delegard (1997) provide a good discussion of the reasons they believe that plutonium was co-precipitated with iron or aluminum in Hanford waste tanks.

**Table 10: Molar ratios of Pu-239, U-238, Tc-99, and Np-237 to Fe in F-Area Tanks 19 and 20.**

| Tank | Pu-239/Fe | U-238/Fe | Tc-99/Fe | Np-237/Fe |
|---|---|---|---|---|
| 19* (core sample) | $5x10^{-5}$ | $2x10^{-2}$ | $2x10^{-4}$ | 2x10-6 |
| 20** | $4x10^{-5}$ | $5x10^{-3}$ | $4x10^{-4}$ | 3x10-6 |

* - from Swingle (2002)

* - from d'Entremont and Hester (1997)

Many of the radionuclides of interest may be co-precipitated with solid iron or other metal hydroxides or oxides in the residual waste. This is supported by concentrations of rare earth elements, often considered surrogates for actinides, in natural iron oxides and oxyhydroxides formed at low temperature environments. For example, Hren et al. (2006) report rare earth element concentrations in low temperature hematite and goethite that range from about 0.1 ppm to 9 ppm (one sample of goethite contained 132 ppm Ce). If all iron and Pu-239 in Tank 19 residual waste resided in hematite the Pu-239 would have a concentration of 1.4 ppm in the hematite. Thus, it is plausible that a large fraction of plutonium and other radionuclides might be in a co-precipitated form. Supporting this idea is that Hobbs (1999) found that both plutonium and uranium co-precipitated with iron under simulated SRS tank conditions. In addition, Gävfert et al. (2002) found that uranium and plutonium were both effectively removed from solution by co-precipitation with iron hydroxides in a water treatment process. Similarly, Slater et al. (1997) describe a method of removing plutonium from waste solutions by co-precipitating it with magnetite. They achieved decontamination factors in the $10^4$ to $10^5$ range and their experimental data suggest a plutonium distribution coefficient on the order of 1000 in the magnetite produced by their experiments. Co-precipitation with iron hydroxides has also been used to quantitatively remove plutonium from liquid samples prior to analysis (Lozano et al., 1997). Thus, it is likely that most of the plutonium and perhaps the uranium in SRS tanks are co-precipitated in iron phases known to be prevalent.

Technetium may also be co-precipitated with iron phases in the waste tanks. Cantrell et al. (2006) observed that a significant fraction of Tc-99 in Hanford waste tank sludge was relatively insoluble, 20% in one sample and 80% in another, and that the insoluble Tc-99 was correlated with iron oxides in selective extraction experiments. Krupka et al. (2009) also observed Tc co-precipitated with ferric iron phases in Hanford tank waste. The experiments of Wakoff and Nagy (2004) further indicate that co-precipitation of Tc in ferric iron phases is likely. They conducted

experiments with perrhenate, an analogue for pertechnitate, under Hanford tank sludge conditions and concluded that up to 14% of the Tc-99 in tank sludges may be irreversibly sorbed, possibly co-precipitated, in iron and aluminum solids. Gu et al. (2003) also hypothesized that Tc-99 was removed from solution during titration experiments of acidic groundwater by co-precipitation with iron and aluminum phases.

There is also evidence in the literature that neptunium may readily co-precipitate with ferric iron oxides. Grigoriev et al. (2001) found that Np(V) and Np(VI) sorb strongly to ferric oxyhydroxides at high pH, while Np(IV) forms true mixed oxide co-precipitates. If neptunium sorbed strongly to ferric iron phases as they formed, and these particles settled to the bottom of the tanks to form a lithified heel, the neptunium would be effectively co-precipitated. Its release to pore fluids would require dissolution of the ferric iron phases. Likewise, Nakata et al. (2002) observed that Np(IV) sorbed strongly on magnetite in anaerobic conditions, while Np(V) sorbed strongly to hematite under aerobic conditions.

It is likely that co-precipitation of Tc, Np, U, and Pu in iron hydroxides/oxides is initiated by adsorption of these radionuclides on particles of ferric iron phases as they precipitate. As the particles grow or become agglomerated into larger masses the radionuclides are effectively co-precipitated – isolated from pore fluid by their entrapment in ferric iron phases. Wakoff and Nagy (2004) suggest that for Tc (they used Re as an analogue), the co-precipitation is by adsorption within the microporosity of precipitating ferrihydrite. As the ferrihydrite recrystallizes to hematite or goethite, the microporosity is closed off and the Tc is isolated from interparticle pore fluids. This is probably also the case for U and Pu because none of these radionuclides fit well into the crystal lattice of ferric iron oxides or hydroxides. Thus, a thermodynamic treatment is not applicable.

Nevertheless, an apparent solubility can be estimated for radionuclides co-precipitated by this mechanism by assuming that the radionuclides are homogenously distributed within the mass of ferric iron phase. This is reasonable if soluble iron was added to the waste stream during or after the radionuclides of interest. Ferrous sulfamate was added during the PUREX process used at SRS to reduce plutonium (Bibler, 1975; Starks, 1977). It is reasonable that this iron precipitated upon pH neutralization prior to disposition in the tanks. Ferric iron precipitated by an increase in pH generally occurs initially as colloidal-sized particles of an amorphous hydroxide. The particles subsequently agglomerate and settle out. With time the amorphous hydroxide becomes increasingly crystalline and usually converts to hematite or goethite. A relatively homogenous distribution of radionuclide within an aged ferric iron phase would be expected if the radionuclide was initially adsorbed to the early colloidal particles. This is the inherent assumption used by Cantrell et al. (2006) to calculate apparent solubility of Tc co-precipitated with iron – that the ratio of the radionuclide to iron in solution as the iron phase is dissolved is equal to the ratio in the solid phase.

Recent work by Smith et al. (2009) suggests that uranium co-precipitated with hydrous ferrous oxides (HFO) becomes less extractable with age as the originally amorphous HFO becomes more crystalline and hematite and goethite begin to crystallize. This is consistent with the observations of Tc leachability when co-precipitated with iron reported by Wakoff and Nagy (2004). However, the work of Smith et al. (2009) also shows that U is preferentially leached

compared to iron when the solid is exposed to extractants. But, it should be noted that their aged iron phase still contained appreciable ferrihydrite. They suggest that the preferential leaching of U by a carbonate extractant may be the result of dissolution of the ferrihydrite with subsequent reprecipitation of the iron. The other possibility they suggest is that the U is not homogenously distributed in the aged particles, but is concentrated near the surface. This is a reasonable explanation considering their aged particles are very small – on the order of 0.2 micrometers. Radionuclide-bearing iron mineral particles present after tank washing are likely to be fused together in much larger agglomerates/crystals or the washing process would remove all of the radionuclide. Thus, on the sub-micrometer scale radionuclides may not be homogenously distributed in iron minerals, but on larger scales can be considered to be homogenously distributed for modeling purposes. If future characterization of residual tank waste shows different, the co-precipitation model can be updated.

Table 11 lists calculated apparent solubilities in the non-submerged tanks of F-Area for uranium, plutonium, technetium, and neptunium co-precipitated with hematite under oxidizing conditions and magnetite under reducing conditions. Reducing Region II, Oxidizing Region II, and Oxidizing Region III conditions are shown. It was also assumed that the ratios of radionuclide to iron in solution equaled those measured in the tank residual waste. Data on radionuclide and iron concentrations in the tanks was from Swingle (2002) and d'Entremont and Hester (1997). Based on calculated grout degradation curves (Appendix B), Reduced Region III will not exist because the reducing capacity of the grout will be exhausted before the transition from Region II to Region III.

**Table 11: Apparent solubilities (moles/L) of co-precipitated Pu-239, U-238, Tc-99, and Np-237 in residual waste for the non-submerged tanks in F-Area.**

| Radionuclide | Tank | Red. Reg. II | Ox. Reg. II | Ox Reg. III |
|---|---|---|---|---|
| Pu-239 | 19 | 2 E-14 | 2 E-15 | 6 E-17 |
| | 20 | 1 E-14 | 2 E-15 | 5 E-17 |
| U-238 | 19 | 7 E-12 | 9 E-13 | 2 E-14 |
| | 20 | 2 E-12 | 2 E-13 | 6 E-15 |
| Tc-99 | 19 | 7 E-14 | 9 E-15 | 2 E-16 |
| | 20 | 1 E-13 | 2 E-14 | 5 E-16 |
| Np-237 | 19 | 7 E-16 | 9 E-17 | 2 E-18 |
| | 20 | 1 E-15 | 1 E-16 | 4 E-18 |

The choices of hematite (oxidized conditions) and magnetite (reduced conditions) as the carrier phases for co-precipitated radionuclides are reasonable. Iron phases identified in Hanford tank residual waste include hematite, goethite, and maghemite (Krupka et al., 2009). Cantrell et al. (2008) identified hematite as a dominant iron phase in tank 241-C-103. Yet, if goethite was the dominant carrier phase under oxidizing conditions, the apparent solubilities would be approximately 3 times higher than those calculated for hematite as the carrier phase.

Analyses of representative H-Area residual tank waste samples were not available to determine the radionuclide to iron ratios. Therefore, calculations of apparent solubilities of co-precipitated U, Pu, Tc, and Np were based on analysis of the Waste Characterization System (Tran, 2007). A radionuclide to iron ratio was calculated for each tank based on the Waste Characterization System. Solubilities of each radionuclide of interest for each H-Area tank were calculated from

these ratios and the solubility of iron at the different pore fluid compositions of interest. The median, maximum, and minimum apparent solubilities in non-submerged H-Area tanks are reported in Table 12. Similar information for the partially submerged tanks in H-Area is shown in Table 13.

**Table 12: Summary of apparent solubilities (moles/L) of co-precipitated radionuclides in non-submerged H-Area tanks.**

| | | Porewater Conditions | | |
|---|---|---|---|---|
| **Element** | | **Red. Reg. II** | **Ox. Reg. II** | **Ox. Reg. III** |
| **U** | Median (molar) | 7 E-12 | 9 E-13 | 2 E-14 |
| | Maximum | 2 E-10 | 2 E-11 | 5 E-13 |
| | Minimum | 4 E-15 | 6 E-16 | 1 E-17 |
| **Pu** | Median | 7 E-14 | 9 E-15 | 2 E-16 |
| | Maximum | 9 E-13 | 1 E-13 | 3 E-15 |
| | Minimum | 4 E-15 | 5 E-16 | 1 E-17 |
| **Tc** | Median | 6 E-13 | 7 E-14 | 2 E-15 |
| | Maximum | 2 E-12 | 2 E-13 | 6 E-15 |
| | Minimum | 1 E-14 | 2 E-15 | 4 E-17 |
| **Np** | Median | 2 E-14 | 2 E-15 | 5 E-17 |
| | Maximum | 4 E-14 | 5 E-15 | 1 E-16 |
| | Minimum | 3 E-17 | 3 E-18 | 8 E-20 |

**Table 13: Summary of apparent solubilities (moles/L) of co-precipitated radionuclides in partially submerged H-Area tanks.**

| | | Submerged Porewater Conditions | | | |
|---|---|---|---|---|---|
| **Element** | | **A** | **B** | **C** | **D** |
| **U** | Median (molar) | 9 E-12 | 3 E-14 | 8 E-12 | 6 E-14 |
| | Maximum | 2 E-11 | 8 E-14 | 2 E-11 | 1 E-13 |
| | Minimum | 2 E-13 | 5 E-16 | 1 E-13 | 1 E-15 |
| **Pu** | Median | 1 E-13 | 4 E-16 | 8 E-14 | 7 E-16 |
| | Maximum | 3 E-12 | 1 E-14 | 3 E-12 | 2 E-14 |
| | Minimum | 1 E-14 | 5 E-17 | 1 E-14 | 1E-16 |
| **Tc** | Median | 8 E-13 | 3 E-15 | 7 E-13 | 5 E-15 |
| | Maximum | 1 E-10 | 4 E-13 | 1 E-10 | 8 E-13 |
| | Minimum | 2 E-13 | 8 E-16 | 2 E-13 | 1 E-15 |
| **Np** | Median | 2 E-14 | 8 E-17 | 2 E-14 | 2 E-16 |
| | Maximum | 7 E-14 | 3 E-16 | 6 E-14 | 5 E-16 |
| | Minimum | 6 E-15 | 2 E-17 | 5 E-15 | 4 E-17 |

Condition A: Porewater = Groundwater
Condition B: Porewater = Groundwater equilibrated with calcite
Condition C: Porewater = Mixture 0.9 Groundwater + 0.1 Reduced Region II Porewater
Condition D: Porewater = Mixture 0.9 Groundwater + 0.1 Oxidized Region II Porewater

The assumption that radionuclide release is controlled by solubility of discrete radionuclide phases rather than co-precipitation is conservative if equilibrium prevails and the choice of solubility controlling minerals is biased towards those with high solubility. This is because apparent solubility from a co-precipitated form only controls the release of the radionuclide to solution if it does not exceed the solubility of the selected discrete phase. Otherwise, the solubility of the selected discrete phase controls radionuclide release.

## Affect of Partial Pressure of Carbon Dioxide ($PCO_2$) on Solubility

Several elements are known to form aqueous carbonate complexes at elevated pH. Those that have radionuclides with high inventories in the F-Area tanks and long half-lives that are known to form aqueous carbonate complexes are plutonium, neptunium, uranium, and americium. At a constant elevated pH, as $PCO_2$ increases the solubility of these elements will increase. $PCO_2$ was considered differently in calculation of solubilities in Bradbury and Sarott's Regions II and III. In Region II it was assumed that $PCO_2$ would be very low, controlled by the reaction of $CO_2$ with portlandite producing calcite. This was modeled by assuming the infiltrating pore fluid was in equilibrium with atmospheric $CO_2$ prior to contact with the tank grout. As it passes through the grout more and more $CO_2$ is removed from solution, and thus the gas phase, by precipitation of calcite. For Region III, where the grout is completely carbonated, it was assumed that the radionuclide solubility reactions were at the $PCO_2$ of the atmosphere, because there is no reaction to remove $CO_2$ as infiltrate passes through the grout.

It is possible, though, that the $PCO_2$ at the CZ is influenced by soil $PCO_2$ that is typically higher than atmospheric. A sample from a water table well in the vicinity of F-Area was in equilibrium with a calculated $PCO_2$ of $10^{-2.6}$ atm. rather than the atmospheric $PCO_2$ of $10^{-3.5}$ atm. (Strom and Kaback, 1992). This $PCO_2$ is typical of groundwater in water table aquifers at the Savannah River Site in which there is little organic matter to drive the $PCO_2$ values higher. To evaluate how the elevated $PCO_2$ affects the solubility of plutonium, neptunium, uranium, and americium curves of solubility versus $PCO_2$ were calculated. The calculations were done using The Geochemist's Workbench® (Bethke, 1995) and assuming that the CZ is a mixing zone of infiltrate from the grout and $CO_2$ gas diffusing from soil. The rate that $CO_2$ diffuses into the CZ relative to the rate of infiltrate advection and/or ion diffusion from the grout may result in different $PCO_2$ values at steady state. Thus, the composition of the pore fluid in the CZ was assumed to be the same as that in the original solubility calculations, but the $PCO_2$ was varied up to $PCO_2=10^{-2}$ atm. Reaction of $CO_2$ with the infiltrate produces calcite and lowers the pH by the overall reaction:

$$CO_2(aq) + Ca^{+2} = CaCO_3 + 2H^+$$

At a $PCO_2$ of $10^{-2.6}$ atm., the system had equilibrium pH values that ranged from about 7.3 to 7.7, depending on the original chemical state of the infiltrate listed in Table 2 . The calculated curves for Region II infiltrate are shown in Figure 8. The curves for Region III are not shown because the variation in solubilities of the four elements is less than an order of magnitude. This is because the assumed $PCO_2$ in Region III was already at $PCO_2=10^{-3.5}$ atm.

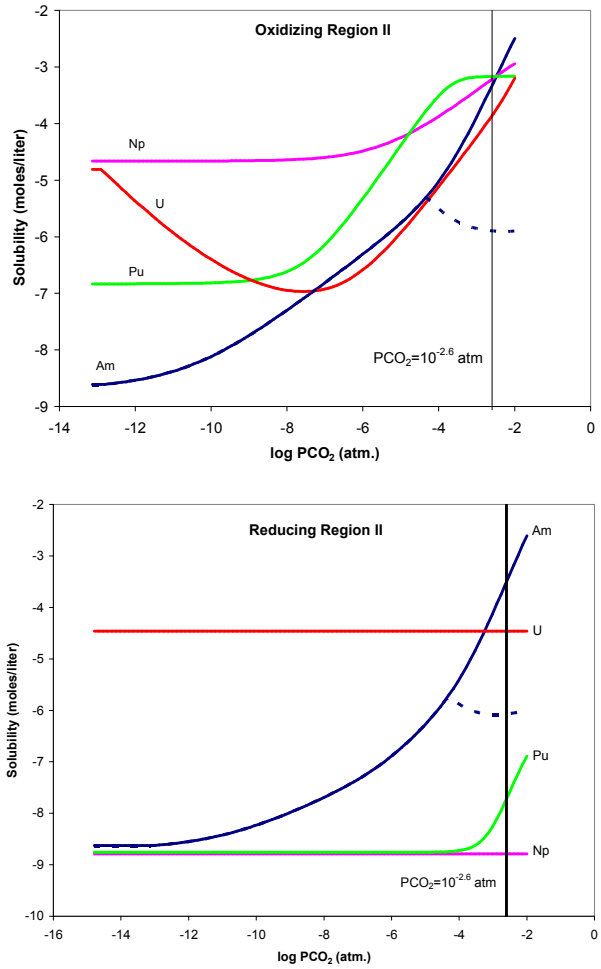


**Figure 8: Calculated solubility curves for uranium, plutonium, neptunium, and americium versus $PCO_2$. Dashed line is solubility of americium allowing carbonate phases to precipitate.**

The solubilities of uranium, plutonium, neptunium, and americium are most affected in the oxidizing chemical state, because known aqueous carbonate complexes are more influential at oxidizing conditions. Table 4 shows the solubilities at a $PCO_2$ of $10^{-2.6}$ atm compared to the original calculated values. The solubility of plutonium increases 3 orders of magnitude under oxidizing conditions and that of americium increases by about 5 orders of magnitude. The solubilities of uranium and neptunium increase by less than about 1.5 orders of magnitude. Under reducing conditions the solubilities of uranium and neptunium do not increase as $PCO_2$ increases and that of plutonium increases by less than an order of magnitude. The solubility of americium increases by 5 orders of magnitude under reducing conditions. However, if carbonate phases of americium are allowed to precipitate the increases in solubility under both oxidizing and reducing conditions is much less (the dashed lines in Figure 8).

**Table 14: Comparison of solubilities originally calculated (Table 4) to those when $PCO_2$ is constant at $10^{-2.6}$ atm.**

| Element | Original Solubility from Table 4 (moles/L) | Solubility at $PCO_2=10^{-2.6}$ atm. (moles/L) |
|---|---|---|
| **Oxidizing Region II** | | |
| Uranium | 3.4E-7 | 1.5E-4 |
| Plutonium | 3.0E-7 | 6.8E-4 |
| Neptunium | 6.8E-7 | 6.4E-4 |
| Americium | 8.6E-9 | 5.4E-4 ($Am(OH)_3$ |
| | | 1.3E-6 ($Am_2(CO_3)_3$) |
| | | 3.2E-7 ($AmOHCO_3$) |
| **Reducing Region II** | | |
| Uranium | 3.5E-5 | 3.5E-5 |
| Plutonium | 1.7E-9 | 1.7E-8 |
| Neptunium | 4.8E-9 | 1.6E-9 |
| Americium | 8.8E-9 | 2.8E-4 ($Am(OH)_3$) |
| | | 8.5E-7 ($Am_2(CO_3)_3$) |
| | | 2.5E-7 ($AmOHCO_3$) |

Precipitation of calcite during equilibration with elevated soil $PCO_2$ values may eventually occlude porosity around the CZ and limit waste release. About 0.5 $cm^3$ of calcite is precipitated for each liter of pore fluid equilibrated with a $PCO_2$ of $10^{-2.6}$ atm. Therefore, after a few hundred pore volumes of infiltrate equilibrate with the elevated $PCO_2$ the porosity may be completely occluded.

## *Chemical Degradation of Reducing Grout*

Evolution of the chemical conditions in the grout was modeled using The Geochemist's Workbench® (Bethke, 2005). Details of these calculations are presented in Appendix B. The first step was to estimate the hydrated mineralogy of the reducing grout from the grout formula presented in the Performance Objective Demonstration Document (PODD) (Buice et al., 2005). This formula together with chemical compositions of the grout components allowed calculation of the final chemical composition of the reducing grout. From this composition, a normative mineralogy was estimated by assuming all calcium was in the phase CSH (calcium silicate

hydrate), all magnesium in hydrotalcite, excess aluminum was in gibbsite, and that remaining silica was inert to pore fluids. The amount of pyrrhotite in the reducing grout was estimated from the measured reducing capacity of the slag (Kaplan et al., 2005), the amount of slag, and the reaction:

$$FeS + 2O_{2(aq)} = Fe^{+2} + SO_4^{-2}$$

Table 15 presents the grout formula and the estimated hydrated mineralogy used in the model.

**Table 15: Reducing grout formula and estimated hydrated mineralogy.**

| Reducing Grout Formula | | Estimated Hydrated Mineralogy | |
|---|---|---|---|
| **Grout Component** | **Amount (lbs/yd$^3$)** | **Mineral** | **Amount (g/m$^3$)** |
| Portland Cement | 75 | CSH | 192583 |
| Class F Fly Ash | 375 | Hydrotalcite | 47475 |
| Slag | 210 | Gibbsite | 50505 |
| Quartz Sand | 2300 | Pyrrhotite | 967 |
| Water | 501 | | |

For the non-submerged tanks the grout mineralogy in Table 15 was reacted with an infiltrate calculated to simulate rainwater passing through a kaolinitic soil assuming no interaction with tank capping materials. For the submerged tanks the grout mineralogy was reacted with a groundwater composition obtained from a well near the H-Area Tank Farm. The reactions were done in the "flush" mode meaning as water enters the block of grout it pushes out an equivalent volume of water that has equilibrated with the grout. The simulations were done in two steps because the model becomes unstable and terminates at the abrupt change in Eh when reducing capacity is exhausted. This results in minor inconsistencies between the end of the first step and the beginning of the second. The results for the non-submerged and submerged tanks are shown in Figure 9 and Figure 10. Table 16 provides a summary of the number of pore volumes of infiltrate required to bring about the various step changes in pore fluid conditions for the non-submerged and submerged tanks.

**Table 16: Summary of grout degradation simulations; pore volumes of infiltrate reacted required to cause step changes in chemical conditions.**

| Tank Position | Transition | Pore Volumes |
|---|---|---|
| Non-Submerged | Reduced Region II to Oxidized Region II | 371 |
| | Oxidized Region II to Oxidized Region III | 2131 |
| Submerged | Condition C to Condition D | 1414 |
| | Condition D to Oxidized Region III | 2383 |

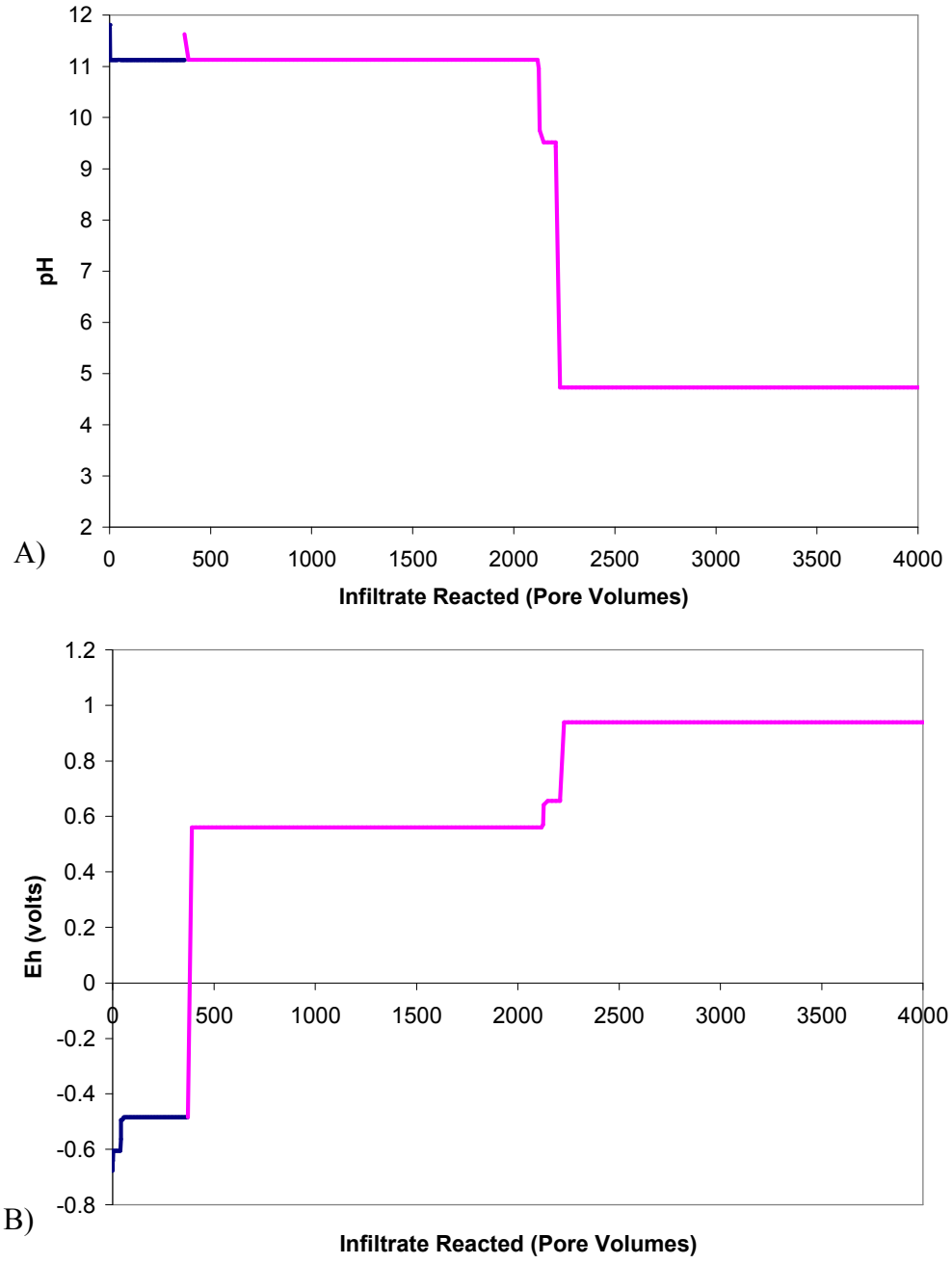


**Figure 9: Pore fluid pH (A) and Eh (B) during simulated degradation of reduced tank grout of non-submerged tanks.**

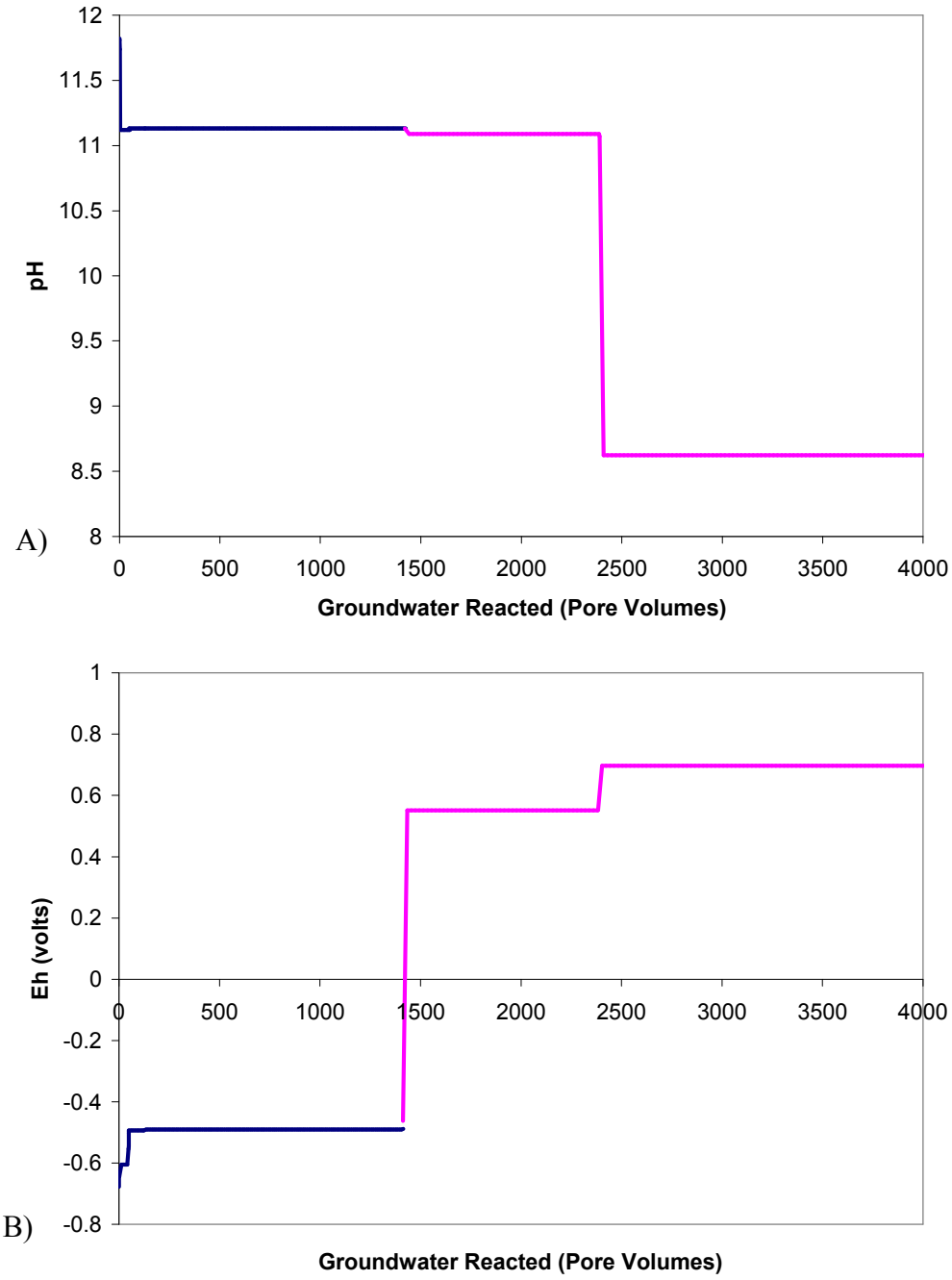


**Figure 10: Pore fluid pH (A) and Eh (B) during simulated degradation of reduced tank grout of submerged tanks.**

## Comparison to Other Studies

The chemical environment in a closed tank is fairly unique and waste release models from other waste forms are not necessarily comparable. For example, solubilities calculated for WIPP (Hobart et al., 1996) and the Yucca Mountain Project (Bechtel, 2005; Cohen & Associates, 2006) are not comparable to solubilities calculated here because chemical conditions at these waste site are different than waste in a reducing cementitious environment. Peretrukhin et al. (1995) discussed release of radionuclides from alkaline waste sludges, a condition similar to that prior to closure of the tanks. Harmsen and Schulz (1998) examined radionuclide release from Hanford tank sludges, but did not consider the post-closure environment. Likewise, Deutsch et al. (2005) and Cantrell et al. (2006) discussed waste release from Hanford tanks, but not under cementitious reducing conditions. Deutsch et al. (2006) did consider waste release from Hanford tanks under cementitious conditions using empirical release rates developed from laboratory leaching experiments. ORNL (1997) reported solubilities of radionuclides from cementitious waste forms as well. Neither of these considered reducing conditions, but the release concentrations reported may be compared to Oxidizing Region II solubilities reported here and are shown in Table 4.

**Table 17: Comparison of release concentrations (moles/liter) of this study to two other studies of cementitious waste forms.**

| Element | Oxidizing Region II | ORNL (1997) | Deutsch et al. (2006) |
|---|---|---|---|
| U | 3.4E-7 | 1.5E-6 | 1.5E-7 |
| Np | 6.8E-7 | 4.0E-5 | - |
| Pu | 3.0E-7 | 1.7E-8 | - |
| Am | 8.6E-9 | 3.3E-6 | - |
| Tc | No solubility control | 9.1E-2 | 1.2E-8 |

With the exception of Tc-99, the release concentrations are generally consistent. In this study, Tc-99 was assumed to have no solubility control under oxidizing conditions. The release concentration reported by Deutsch et al. (2006) was derived from leaching of Hanford waste with simulated cementitious pore fluid. That the value from Deutsch et al. (2006) is several orders of magnitude lower than the solubility reported in ORNL (1997) suggests that Tc-99 in Hanford waste tanks is held in a form other than a discrete technetium phase.

The best compilation of solubility data that is comparable to the solubilities estimated here is Kaplan (2006). He used a compilation of Performance Assessment data for cementitious waste by McDowell-Boyer et al. (2000) and other literature sources to develop solubilities for radionuclides in cementitious environments. The “young cement” values are comparable to Region II values in this study. The “moderately aged” values and the “aged” cement values are at different pH values than used in this study for Region III cements. Selected young cement values of Kaplan (2006) and those of Region II in this study are shown in Table 18 for comparison. For

the most part, the solubility values from this study are comparable but a bit higher than those presented in Kaplan (2006). The two exceptions are for Tc and Np under reducing conditions.

**Table 18: Comparison of solubilities calculated in this study to those presented in Kaplan (2006).**

| Element | Kaplan (2006) Oxidizing (moles/L) | Region II Oxidizing (moles/L) | Kaplan (2006) Reducing (moles/L) | Region II Reducing (moles/L) |
|---|---|---|---|---|
| U | $10^{-7}$ | 3.4E-7 | $10^{-6}$ | 3.5E-5 |
| Np | $10^{-8}$ | 6.8E-7 | $10^{-6}$ | 4.8E-9 |
| Pu | $10^{-8}$ | 3.0E-7 | $10^{-10}$ | 1.7E-9 |
| Am | $10^{-11}$ | 8.6E-9 | $10^{-11}$ | 8.8E-9 |
| Tc | None | None | $10^{-10}$ | 1.2E-32 |

# References

Atkins, M., A.N. Beckley, and F.P. Glasser, 1988. Influence of cement on the near field environment and its specific interactions with uranium and iodine. *Radiochimica Acta*, 44/45, 255-261.

Atkins, M., F.P. Glasser, and A. Kindness, 1992a. "Cement Hydrate Phases: Solubility at 25$^{o}$C." *Cement and Concrete Research*, 22, 241-246.

Atkins, M., D.G. Bennett, A.C. Dawes, F.P. Glasser, A. Kindness, and D. Read, 1992b. "A thermodynamic model for blended cements." *Cement and Concrete Research*, 22, 497-502.

Bechtel, 2005. Dissolved Concentration Limits of Radioactive Elements. ANL-WIS-MD-000010, Rev. 5, Bechtel SAIC Company, Las Vegas, NV.

Barney, G.S. and C.H. Delegard, 1997. Chemical Species of Plutonium in Hanford Radioactive Tank Waste. HNF-SA-3181-FP, B&W Hanford Company, Richland, WA.

Bennett, D.G., D. Read, M. Atkins, and F.P. Glasser, 1992. A thermodynamic model for blended cements. II: Cement hydrate phases; thermodynamic values and modelling studies. *Journal of Nuclear Materials*, 190, 315-325.

Berner, U.R., 1988. Modelling the incongruent dissolution of hydrated cement minerals. *Radiochimica Acta*, 44/45, 387-393.

Bethke, C.M., 2005, The Geochemist's Workbench® (geochemical modeling software), Release 6.0, University of Illinois.

Bibler, N.E., 1975. Radiolytic Instability of Ferrous Sulfamate in Nuclear Process Solutions. DP-MS-75-56, E.I. du Pont de Nemours & Co., Aiken, SC.

Bradbury, M. H., Sarott, F., 1995. Sorption Database for the Cementitious Near-Field of a L/ILW Repository for Performance Assessment, PIT-MISC-0075, ISSN 1019-0643, Paul Scherrer Institut, Switzerland.

Buice, J.M., R.K. Cauthen, R.R. Haddock, B.A. Martin, J.A. McNeil, J.L. Newman, and K.H. Rosennberger, 2005. Performance Objective Demonstration Document (PODD) for the Closure of Tank 19 and Tank 18 Savannah River Site. CBU-PIT-2005-00106, Westinghouse Savannah River Company, Aiken SC.

Caldwell, T.B., 1997. Tank Closure Reducing Grout. WRSC-TR-97-0102, Westinghouse Savannah River Company, Aiken SC.

Cantrell, K.J., K.M. Krupka, W.J. Deutsch, and M.J. Lindberg, 2006. Residual waste from Hanford tanks 241-C-203 and 241-C-204. 2. Contaminant Release Model, *Environmental Science and Technology*, 40, 3755-3761.

Cantrell, K.J., K.M. Krupka, W.J. Deutsch, M.J. Lindberg, H.T. Schaef, K.N. Geiszler, and B.W. Arey, 2008. Hanford Tank 241-C-103 Residual Waste Contaminant Release Models and Supporting Data. PNNL-16738, Pacific Northwest National Laboratory, Richland WA.

Casas, I., J. Bruno, E. Cera, R.J. Finch, and R.C. Ewing, 1997. Characterization and dissolution behavior of a becquerelite from Shinkolobwe, Zaire. *Geochmica et Cosmochimica Acta*, 61, 3879-3884.

Concrete Technology Today, 1999. Volume 20, number 2, August. Portland Cement Association. URL http://www.cement.org/tech/pdfs/pl992.pdf.

Cohen & Associates, 2006. Final Report -- Support to the Revision of 40CFR Part 197 ("Yucca Mountain"), Task 4 – Modeling Uncertainty Effects on a Reference Dose Level. Contract Number EP-D-05-002, U.S. Environmental protection Agency, Washington, DC.

d'Entremont, P.D. and J.R. Hester, 1997. Characterization of Tank 20 Residual Waste. WSRC-TR-96-0267, Westinghouse Savannah River Company, Aiken, SC.

Deustch, W.J., K.M. Krupka, M.J. Lindberg, K.J. Cantrell, C.F. Brown, H.T. Schaef, 2005. Hanford Tank 241-C-106: Residual Waste Contaminant Release Model and Supporting Data. PNNL-15187, Rev. 1, Pacific Northwest National Laboratory, Richland, WA.

Deutsch, W.J., K.M. Krupka, M.J. Lindberg, K.J. Cantrell, C.F. Brown, and H.T. Schaef, 2006. Hanford Tank 241-C-106: Impact of Cement Reactions on Release of Contaminants from Residual Waste. PNNL-15544, Pacific Northwest National Laboratory, Richland, WA.

FTF-IP-06, Rev. 0, 2007. F-Tank Farm Estimated Tank Inventory at Closure. Washington Savannah River Company, Aiken, SC.

Gäfvert, T., C. Ellmark, and E. Holm, 2002. Removal of radionuclides at a waterworks. *Journal of Environmental Radioactivity*, 63, 105-115.

Grenthe, I., J. Fuger, R.J.M. Konings, R.J. Lemire, A.B. Muller, C. N-T. Cregu, and H. Wanner, 1992. Chemical Thermodynamics of Uranium. North-Holland, Amsterdam.

Grigoriev, M.S., A.M. Fedoseev, A.V. Gelis, N.A. Budansteva, V.P. Shilov, V.P. Perminov, M.V. Nikonov, and N.N. Krot, 2001. Study of the interaction of Pu(IV) and Np(IV, V, VI) with iron hydroxides to predict the behaviro of actinides in environmental media. Radiochemica Acta, 89, 95-100.

Gupta, S., M. Dubikova, D. French, and V. Sahajwalla, 2007. Effect of CO2 gasification on the transformation of coke minerals at high temperatures. *Energy & Fuels*, 21, 1052-1061.

Gu, B., S.C. Brooks, Y. Roh, and P.M. Jardine, 2003. Geochemical reactions and dynamics during titration of a contaminated groundwater with high uranium, aluminum, and calcium. *Geochimica et Cosmochimica Acta*, 67, 2749-2761.

Hamm, L. and L. Collard, 2010, A Closer Look at HYF Tank elevations Versus Water Table (GSA Flow Model and Well Data Considered. SRNL-L5200-2010-00001, Savannah River National Laboratory, Aiken, SC.

Harmsen, R.W. and W.W. Schulz, 1998. Best-basis Estimates of Solubility of Selected Radionuclides in Sludges in Hanford Single-shell Tanks. HNF-3271, Rev. 0 , Lockheed Martin Hanford Corporation, Richland, WA.

Hay, M.S., 1997. Analysis of Tank 19F Solids by X-ray Diffraction (U). SRT-LWP-97-111. Westinghouse Savannah River Company, Aiken, SC.

Hay, M. S., K. P. Crapse, S. D. Fink, and J. M. Pareizs, 2007. "Characterization and Actual Waste Tests with Tank 5F Samples," WSRC-STI-2007-00192, Rev. 1, Aiken, SC: Savannah River National Laboratory. Washington Savannah River Company.

Hobart, D.E., C.J. Bruton, F.J. Millero, I-M. Chou, K.M. Trauth, and D.R. Anderson, 1996. Estimates of the Solubilities of Waste Element Radionuclides in Waste Isolation Pilot Plant Brines: A Report by the Expert Panel on the Source Term. SAND96-0098, Sandia National Laboratories, Albuquerque, NM.

Hobbs, D.T., 1999. Precipitation of uranium and plutonium from alkaline salt solutions. *Nuclear Technology*, 128, 103-112.

Hren, M.T., D.R. Lowe, M.M. Tice, G. Byerly, C.P. Chamberlain, 2006. Stable isotope and rare earth element evidence for recent ironstone pods within the Archean Barberton greenstone belt, South Africa. *Geochimica et Cosmochimica Acta*, 70, 1457-1470.

Kaplan, D.I., 2006. Geochemical Data Package for Performance Assessment Calculations Related to the Savannah River Site (U). WSRC-TR-2006-00004 Rev. 0, Washington Savannah River Company, Aiken, SC.

Kaplan, D.I., T. Hang, and S. Aleman, 2005. Estimated Duration of the Reduction Capacity within a High Level Waste Tank (U), WSRC-RP-2005-01674, Washington Savannah River Company, Aiken, SC.

Krupka, K.M., K.J. Cantrell, H.T. Schaef, B.W. Arey, S.M. Heald, W.J. Deutsch, and M.J. Lindberg, 2009. Characterization of Solids in Residual Wastes from Single-Shell Tanks at the Hanford Site, Washington, USA. Presentation to Waste Management 2009.

Lemire, R.J., J. Fuger, H. Nitsche, P. Potter, M.H. Rand, J. Rydberg, K. Spahui, J.C. Sullivan, W.J. Ullman, P. Vitorge, and H. Wanner, 2001. Chemical Thermodynamics of Neptunium and Plutonium. North-Holland, Amsterdam.

Lilley, M.S., B.A. Powell, and D.I. Kaplan, 2009. Iodine, Neptunium, Plutonium and Technetium Sorption to Saltstone and Cement formulations Under Oxidizing and Reducing Conditions, SRNL-STI-2009-00626 Rev. 0. Savannah River National Laboratory, Aiken, SC.

Lozano, J.C., F. Fernandez, and J.M.G. Gomez, 1997. Preparation of alpha-spectrometric sources by coprecipitation with Fe(OH)3: Application to actinides. *Applied Radiation and Isotopes.*, 48, 383-389.

Lukens, W.W., J.J. Bucher, D.K. Shuh, and N.M. Edelstein, 2004. Evolution of technetium speciation in reducing grout. *Environmental Science & Technology*, 39, 8064-8070.

Malek, R.I.A., D.M. Roy, M.W. Barnes, and C.A. Langton, 1985. Slag Cement – Low-level Waste Forms at the Savannah River Plant. DP-MS-85-9, E.I. du Pont de Nemours and Company, Aiken SC.

McDowell-Boyer, L., A.D. Yu, J.R. Cook, d. Kocher, E.L. Wilhite, H. Holmes-Burns, and K.E. Young, 2000. Radiological Performance Assessment for the E-Area Low-level Waste Facility, WSRC-RP-94-218, Rev. 1, Westinghouse Savannah River Company, Aiken, SC.

Moroni, L.P. and F.P. Glasser, 1995. Reactions between cement components and U(VI) oxide. *Waste Management*, 15, 243-254.

Muszer, A., 2006. Petrographical and mineralogical characteristics of the metallurgical slag from the Dörschl Furnace (Głocow Foundry, Poland). *Physicochemical Problems of Mineral Processing*, 40, 89-98.

Nakata, K., S. Nagasaki, S. Tanaka, Y. Sakamoto, T. Tanaka, and H. Ogawa, 2002. Sorption and reduction of neptunium(V) on the surface of iron oxides. *Radiochimica Acta*, 90, 665-669.

Noyes, R., 1994. Operations in Environmental Engineering. William Andrews Publishing.

ORNL, 1997. Performance Assessment for the Class L-II Disposal Facility. ORNL/TM-13401, Oak Ridge National Laboratory, Oak Ridge, TN.

Park, J-Y. and B. Batchelor, 2002. General chemical equilibrium model for stabilized/solidified wastes. *Journal of Environmental Engineering*, 128, 653-661.

Peretrukhin, V.F., V.P. Shilov, and A.K. Pikaev, 1995. Alkaline Chemistry of Transuranium Elements and Technetium and the Treatment of Alkaline Radioactive Wastes. WHC-EP-0817, Westinghouse Hanford Company, Richland, WA.

Piatak, N.M., R.R. Seal II, and J.M. Hammarstrom, 2004. Mineralogical and geochemical controls on the release of trace elements from slag produced by base- and precious-metal smelting at abandoned mine sites. *Applied Geochemistry*, 19, 1039-1064.

Phifer, M.A., M.R. Millings, and G.P. Flach, 2006. Hydraulic Property Data Package for the E-Area and Z-Area Soils, Cementitious Materials, and Waste Zones. WSRC-STI-2006-00198, Rev. 0, Washington Savannah River Company, Aiken, SC.

Ramachandran, V.S.; Beaudoin, James J., 2001. Handbook of Analytical Techniques in Concrete Science and Technology.. William Andrew Publishing/Noyes.
Online version available at:
http://knovel.com/web/portal/browse/display?_EXT_KNOVEL_DISPLAY_bookid=265&VerticalID=0

Rai, D., A.R. Felmy, N.J. Hess, V.L. LeGore, and D.E. McCready, 2002. Thermodynamics of the U(VI)-$Ca^{+2}$-$Cl^{-}$ -$OH^{-}$ -H2O system: Solubility product of becquerelite. *Radiochmimica Acta*, 90, 495-503.

Rard, J.A., M.H. Rand, G. Anderegg, and H. Wanner, 1999. Chemical thermodynamics of Technetium. North-Holland, Amsterdam.

Reardon, E.J., 1990. An ion interaction model for the determination of chemical equilibria in cement/water systems., *Cement and Concrete Research*, 20, 175-192.

Sandino, M.C.A. and B. Grambow, 1994. Solubility equilibria in the U(VI)-Ca-K-Cl-H2O System – Transformation of schoepite into becquerelite and compreignacite. *Radiochimica Acta*, 66-7, 37-47.

Slater, S.A., D.B. Chamberalin, A.A. Aase, B.D. Babcock, C.Conner, J. Sedlet, and G.F. Vandegrift, 1997. Optimization of magnetite carrier precipitation process for plutonium waste reduction. *Separation Science and Technology*, 32, 127-147.

Smith, S.C., M. Douglas, D.A. Moore, R.K. Kukkadapu, and B.W. Arey, 2009. Uranium extraction from laboratory-synthesized, uranium-doped hydrous ferric oxides. *Environmental Science & Technology*, 43, 2341-2347.

Starks, J.B., 1977. The PUREX Process. DPSPU 77-11-1, E.I. du Pont de Nemours & Co., Aiken, SC.

Strom, R.N. and D.S. Kaback, 1992. Groundwater Geochemistry of the Savannah River Site and Vicinity (U). WSRC-RP-92-450, Westinghouse Savannah River Company, Aiken SC.

Swingle, R.F., 2002. Characterization of the Tank 19F Closure Grab and Core Samples and the Tank 18F Dip Sample, WSRC-TR-2002-00107, Westinghouse Savannah River Company, Aiken, SC.

Swingle, R.F., 2003. Characterization of the Tank 18F Closure Samples. WSRC-TR-2003-00449, Rev. 0, Westinghouse Savannah River Company, Aiken, SC.

Tran, H.Q., Tank Radioactive and Non-radioactive Inventories (8/14/2007). LWO-LWE-2007-00250, Rev. 0. Westinghouse Savannah River Company, Aiken, SC.

Vochten, R. and L. Van Haverbeke, 1990. Transformation of schoepite into the uranyl oxide hydrates: Becquerelite, billietite, and wölsendorfite. *Mineralogy and Petrology*, 43, 65-72.

Wakoff, B. and K.L. Nagy, 2004. Perrhenate uptake by iron and aluminum oxyhydroxides: An analogue for pertechnetate incorporation in Hanford waste tank sludges. *Environmental Science and Technology*, 38, 1765-1771.

Wellman, D.M., S.V. Mattigod, B.W. Arey, M.I. Wood, and S.W. Forrester, 2007. Experimental limitations regarding the formation and characterization of uranium-mineral phases in concrete waste forms. *Concrete and Cement Research*, 37, 151-160.

Zainoun, K., J. Puziewicz, and H. Bril, 2003. Primary Pb-Zn-bearing phases in pyrometallurgical slag from Świętochłowice (Upper Silesia, Poland). *Mineralogical Society of Poland – Special Papers, 23*.

# Appendix A – Solubility versus Adsorption Controls

The conceptual model for estimating waste release from the CZ assumes the waste release is solubility controlled. This is based on inventories of radionuclides and the volume of waste assumed to remain in the tanks after washing (FTF-IP-06). For uranium isotopes, plutonium isotopes, Tc-99, Np-237, and Am-241, the post-wash inventories per single pore volume are much higher than would be soluble in a single pore volume. More importantly, apparent partition coefficients (Kds) calculated from the post-wash inventories and amount of matrix are generally too high to reasonably conclude that adsorption controls dominate waste release.

The Kd values were calculated by assuming a tank bottom area of 527.2 $m^2$ and a CZ thickness of $1.6x10^{-3}$ m, to give a total post-wash waste volume of 0.84 $m^3$. The porosity of the CZ was assumed to be 21.1%, giving a pore volume (Vp) of 0.18 $m^3$ and a matrix mineral volume of 0.66 $m^3$. The density of the matrix minerals was assumed to be that of hematite, 5.3 $g/cm^3$. Thus, the estimated mass of the CZ ($M_{CZ}$) was assumed to be $3.5x10^6$ grams.

The Kd is defined as:

$$K_d = \frac{C_{solid}}{C_{aqueous}}$$

where $C_{solid}$ is the concentration of the radionuclide in the solid phase and $C_{aqueous}$ is the concentration in the aqueous phase. The inventory in the solid phase is the total inventory minus the inventory in the aqueous phase. For these calculations the inventory in the aqueous phase is defined as the calculated solubility (S) in moles/liter of the radionuclide multiplied by the total fluid pore volume (Vp) in the CZ of a tank. Thus, the Kd in ml/g is defined by:

$$C_{solid}\left(\frac{moles}{g}\right) = \frac{\mathrm{I_T} - 1000\,\mathrm{V_P S}}{\mathrm{M_{CZ}}}$$

and $$C_{aqueous}\left(\frac{moles}{ml}\right) = 0.001S$$

therefore $$K_d\left(\frac{ml}{g}\right) = \frac{I_T - 180S}{3500S}$$

where $I_T$ is the total radionuclide inventory in moles in the CZ and S is the calculated solubility in moles/liter. Table 19 shows the minimum, maximum, and median values of Kd calculated for all F-Area tanks for total uranium, total plutonium, Tc-99, Np-237, and Am-241. The solubility under Reducing Region II conditions was used because it was assumed that these would be the equilibrium conditions when the tank liner is breached and waste first leaches to the environment. Low Kd values occur in a few tanks, particularly for Np-237, because the

inventory in these tanks is low. It is important to note that if adsorption controls were used to estimate waste release rates and the median Kd values were used, the release rates would be slower than those estimated from solubility controls. This is true even if supersaturation of the pore fluids was allowed.

**Table 19: Calculated apparent Kd values in F-Area tanks if adsorption was controlling waste release.**

| Nuclide/Element | Minimum Kd (ml/g) | Maximum Kd (ml/g) | Median Kd (ml/g) |
|---|---|---|---|
| Uranium | $8.6x10^{1}$ | $2.4x10^{4}$ | $2.8x10^{2}$ |
| Plutonium | $6.1x10^{3}$ | $1.8x10^{6}$ | $2.6x10^{4}$ |
| Tc-99 | $1.9x10^{42}$ | $2.4x10^{45}$ | $1.2x10^{44}$ |
| Np-237 | 3.2 | $1.2x10^{5}$ | $2.8x10^{3}$ |
| Am-241 | $4.5x10^{14}$ | $7.0x10^{18}$ | $1.3x10^{16}$ |

# Appendix B – Chemical Degradation of Reducing Grout

Chemical degradation of reducing grout to be used in closing SRS tanks controls the chemical composition of the pore fluids passing through the CZ. This, in turn controls the solubility and contaminant release from the CZ. Simulations were done using The Geochemist's Workbench® to estimate the chemical degradation of the reducing grout. It is important to note that these simulations only address chemical degradation, not physical degradation such as fracturing, permeability changes, etc. The simulations presented here estimate chemical changes as a function of number of pore volumes of infiltrate that react with grout minerals. This is independent of physical degradation, though physical degradation may ultimately affect the rate of chemical degradation by influencing the rate at which infiltration passes through the grout.

The simulations were run using The Geochemist's Workbench® in the "Flush" mode. The flush mode mimics column experiments where for each aliquot of infiltrate that enters the column an equal volume of equilibrated pore fluid exits. For the most part, the flush mode simulations yield step changes in pore fluid composition because they account for only equilibrium. Thus, as soon as a mineral that controls Eh or pH disappears by dissolution, a step change occurs in pore fluid composition. In reality, kinetics, incongruent dissolution, coating of minerals, and heterogeneity in flow rates would result in smoother evolution of pore fluid composition.

The simulations were run in two steps because the large step change in Eh from Reduced Region II to Oxidized Region II renders the program unstable. The first step begins with the first pore volume of infiltrate and ends when the program terminates at the large Eh increase. The second step picks up the results -- mineralogy and pore fluid -- of the first step at the point of termination and continues. The beginning of the second step does not perfectly match the end of the second step, so small inconsistencies in reaction path are seen at the transition of the first step to the second step.

Derivation of grout mineralogy is a fundamental basis for the simulations presented here. There are no quantitative measurements of reducing grout mineralogy, but there are chemical analyses of the components that make up the grout. The formula for the reducing grout was taken from the Buice et al. (2005) and is presented in Table 20.

**Table 20: Grout formula used in degradation simulations.**

| Grout Component | Amount (lbs/yd$^3$) | Weight % |
|---|---|---|
| Portland Cement | 75 | 2.17 |
| Class F Fly Ash | 375 | 10.83 |
| Slag | 210 | 6.07 |
| Quartz Sand | 2300 | 66.45 |
| Water | 501 | 14.48 |

Chemical analyses of the individual components of the grout formula are given in Table 21. The chemical composition of the bulk grout was then calculated from the formula and the compositions of the individual components and is presented in Table 22. The analyses of the

individual grout components are from the references listed below Table 21. The exception is that pyrrhotite was added to the slag based on reducing capacity measurements by Kaplan et al. (2005).

The phase in the slag responsible for its reducing properties was assumed to be pyrrhotite with a stoichiometric formula of FeS. Pyrrhotite is a high temperature reduced phase potentially formed under conditions expected during the formation of blast furnace slag and has been identified in various smelting slags (Zainoun et al., 2003; Muszer, 2006; Gupta et al., 2007). The amount of pyrrhotite in the slag was assigned based on slag reducing capacity measurements by Kaplan et al. (2005). They measured a reduction capacity of 0.82 meq/g for slag to be used in tank closure. Based on the oxidation reaction of pyrrhotite:

$FeS + 2O_2(aq) = Fe^{+2} + SO_4^{-2}$

there are 8000 meq of electrons transferred per mole of pyrrhotite or 91 meq/g FeS. From this, the measured reducing capacity of the slag, and the amount of slag used in the grout formula, it was calculated that there were 967 grams of pyrrhotite per cubic meter of grout.

**Table 21: Chemical composition of reducing grout components.**

| Constituent | Class II Cement[a] | Class F Fly Ash[b] | Slag[b] | Quartz Sand |
|---|---|---|---|---|
| $SiO_2$ (wt.%) | 21.2 | 52.17 | 34.70 | 100 |
| $Al_2O_3$ | 4.6 | 27.60 | 10.70 | 0 |
| $Fe_2O_3$ | 3.5 | 4.36 | 0 | 0 |
| CaO | 63.8 | 0.96 | 39.37 | 0 |
| MgO | 2.1 | 0.61 | 11.90 | 0 |
| $SO_3$ | 2.7 | 9.92 | 0 | 0 |
| $H_2O$ | 0 | 0 | 0 | 0 |
| FeS | 0 | 0 | 0.84[c] | 0 |

a – Type II Mean from Concrete Technology Today (Aug., 1999)
b – Malek et al. (1985)
c – calculated from data in Kaplan et al. (2005); explained in text

**Table 22: Calculated chemical composition of reducing grout.**

| Constituent | Bulk Reducing Grout (moles/kg) |
|---|---|
| $SiO_2$ | $1.24 \times 10^{1}$ |
| $Al_2O_3$ | $3.66 \times 10^{-1}$ |
| $Fe_2O_3$ | $3.43 \times 10^{-2}$ |
| CaO | $6.97 \times 10^{-1}$ |
| MgO | $2.08 \times 10^{-1}$ |
| $SO_3$ | $1.41 \times 10^{-1}$ |
| $H_2O$ | 8.06 |
| FeS | $5.80 \times 10^{-3}$ |

To estimate reducing grout mineralogy, a normative calculation was done that assigned chemical constituents from the bulk composition in Table 22 to specific mineral phases. The normative mineralogy calculation method of Atkins et al (1992a) is not applicable to calcium poor systems such as the proposed tank grout. In the third step of Atkins et al. (1992a), the apportioning of remaining aluminum and calcium, the composition lies outside of the $SiO_2$-$Al_2O_3$-$Ca(OH)_2$ ternary diagram provided by Atkins et al. (1992a). The normalized remaining $Ca(OH)_2$ is 20 molar%. Hence, for the grout degradation simulations presented here all calcium was assigned to CSH, all magnesium was assigned to hydrotalcite, all FeS was assigned to pyrrhotite, and all $Fe_2O_3$ was assigned to hematite. Left over aluminum was assigned to gibbsite, left over silica was assigned to quartz, and left over sulfur was ignored. For use in The Geochemist's Workbench®, hematite, and quartz were assigned to an inert phase so that the final mineralogical composition was that presented in Table 23.

**Table 23: Calculated bulk mineralogical composition of reducing grout.**

| Grout Mineral | Concentration (grams/$m^3$) |
|---|---|
| CSH | 192583 |
| Hydrotalcite | 47475 |
| Pyrrhotite | 967 |
| Gibbsite | 50504 |
| Inert | 1718115 |

Thermodynamic data for several cement phases were entered into the "thermo.dat" database provided with The Geochemist's Workbench®. The dissolution reactions for these, the log of the equilibrium constants for these reactions, and the references from which these data were derived are listed in Table 24. CSH has a variable formula and thus a variable dissolution reaction and free energy of dissolution. For these calculations, the CSH dissolution model of Berner (1988) as presented by Park and Batchelor (2002) was used. In this model CSH is considered as a non-ideal mixture of two solid phases, the identity of which, and their respective dissolution constants, depend on the Ca/Si ratio of the CSH. Here the Ca/Si ratio was assumed to be low, Ca/Si = 0.5, because of the low amount of portlandite relative to fly ash and slag used in the grout. This Ca/Si ratio is at the low end of possible CSH compositions, but as shown in Figure 11 the pH values calculated are not particularly sensitive to Ca/Si ratios up to a ratio of 1.

**Table 24: Thermodynamic data entered into database of The Geochemist's Workbench®.**

| Cement Phase | Dissolution Reaction | log K | Reference |
|---|---|---|---|
| CSH* | $CaSiO_3 \cdot H_2O + 2H^+ = Ca^{+2} + SiO_{2(aq)} + 2H_2O$ | 15.15 | Park and Batchelor (2002) |
| Hydrotalcite | $Mg_4Al_2O_7 \cdot 10H_2O + 14H^+ = 4Mg^{+2} + 2Al^{+3} + 17H_2O$ | 73.78 | Bennett et al. (1992) |
| C4AH13 | $Ca_4Al_2O_7 \cdot 13H_2O + 14H^+ = 4Ca^{+2} + 2Al^{+3} + 20H_2O$ | 100.77 | Reardon (1990) |
| Ca-carboaluminate | $Ca_2Al_2O_4CO_3 \cdot 11H_2O + 9H^+ = 2Ca^{+2} + 2Al^{+3} + HCO_3^- + 15H_2O$ | 34.76 | Reardon (1990) |
| Ettringite | $Ca_6Al_2O_6(SO_4)_3 \cdot 32H_2O + 12H^+ = 6Ca^{+2} + 2Al^{+3} + 3SO_4^{-2} + 38H_2O$ | 57.15 | Reardon (1990) |

* -- see explanation in text

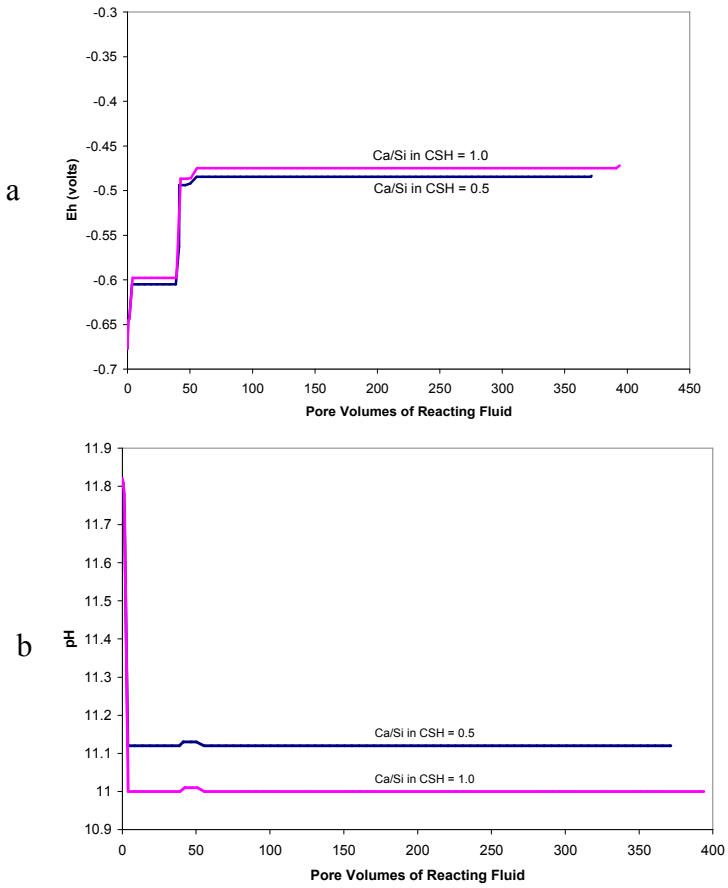


**Figure 11: Effect of assumed Ca/Si ratio of CSH on Eh (a) and pH (b).**

For the non-submerged tanks the infiltrate reacted with the tank grout was the composition of average rainfall in the SRS area reported by Strom and Kaback (1992) equilibrated with kaolinite to simulate reaction with soil. The dissolved oxygen concentration was determined by equilibrating with atmospheric air. The resulting infiltrate composition is reported in Table 25 . The infiltrate was reacted with 1 cubic meter of reducing grout with a porosity of 21.1% (Phifer et al., 2006). At an assumed pore fluid density of 1.013 g/cm3, the mass of a single pore volume of fluid is 208 kg.

**Table 25: Chemical composition of reacting infiltrate.**

| Constituent | Concentration |
|---|---|
| pH | 4.67 |
| $O2_{(aq)}$ | $2.5x10^{-4}$ moles/liter |
| $CO_{2(aq)}$ | $1.1x10^{-5}$ |
| $SO_4^{-2}$ | $1.3x10^{-5}$ |
| $Cl^-$ | $9.9x10^{-6}$ |
| $Na^+$ | $8.7x10^{-6}$ |
| $Ca^{+2}$ | $2.1x10^{-6}$ |
| $Mg^{+2}$ | $1.3x10^{-6}$ |

For the submerged tanks, the infiltrate was a groundwater composition from well P27D (Strom and Kaback, 1992) screened in the water table and located approximately 450 meters east of Tank 43. The composition of this groundwater is shown in Table 26. The groundwater was reacted with the reducing grout using the same grout parameters as discussed above for the non-submerged tanks.

**Table 26: Composition of groundwater from well P27D used as infiltrate to submerged tank grout.**

| Constituent | Concentration |
|---|---|
| pH | 5.4 |
| $O_{2(aq)}$ moles/liter | $3.84 \times 10^{-5}$ |
| $Ca^{+2}$ | $6.24 \times 10^{-5}$ |
| $Mg^{+2}$ | $1.65 \times 10^{-5}$ |
| $Na^{+}$ | $4.35 \times 10^{-5}$ |
| $CO_{2(aq)}$ | $9.84 \times 10^{-5}$ |
| $SO_4^{-2}$ | $6.25 \times 10^{-6}$ |
| $Cl^{-}$ | $8.46 \times 10^{-5}$ |

The grout degradation simulations were run in two steps because the program terminates at the abrupt and large change in Eh that occurs when reduction capacity of the grout is exhausted. The second step begins with the grout mineralogy and pore water composition at the point of termination of the first step. The result is small inconsistencies between the results of the end of the first step and the beginning of the second step.

The second step simulations were run with the grout minerals hydrotalcite and Ca-carboaluminate suppressed – removed from the system – so that calcite would control pH once CSH was completely dissolved. If hydrotalcite is present it constrains pH of Region III to 9.4. Carbonation of cement to $CaCO_3$ is a well documented process (Ramachandran and Beaudoin, 2001) and the pH in Region III is assumed to be dominated by $CaCO_3$. Therefore, in this document pore fluid in Region III of grout degradation is set to conditions of equilibrium with calcite ($CaCO_3$) rather than hydrotalcite or Ca-carboaluminate.

Figure 12 shows the simulated pH and Eh of pore fluids during degradation of the non-submerged tank grout. The pH begins at 11.1, Region II, and stays constant until the transition to Region III at 2131 pore volumes of infiltrate reacted. Calcite is not stable in this simulation and

the pH drops to the infiltrate pH of 4.7. Nevertheless, in the solubility calculations pore fluids in Region III were assumed to be in equilibrium with calcite at a pH of 8.3. The alternative is to assume that hydrotalcite does truly control pH at 9.4. Figure 13 shows the same simulation but with hydrotalcite allowed to be present and react. The transition from Region II to Region III occurs at the same point, 2131 pore volumes, but the pH drops to 9.4 where it remains constant for 4000 pore volumes. Radionuclide solubilities under conditions C and D for the submerged

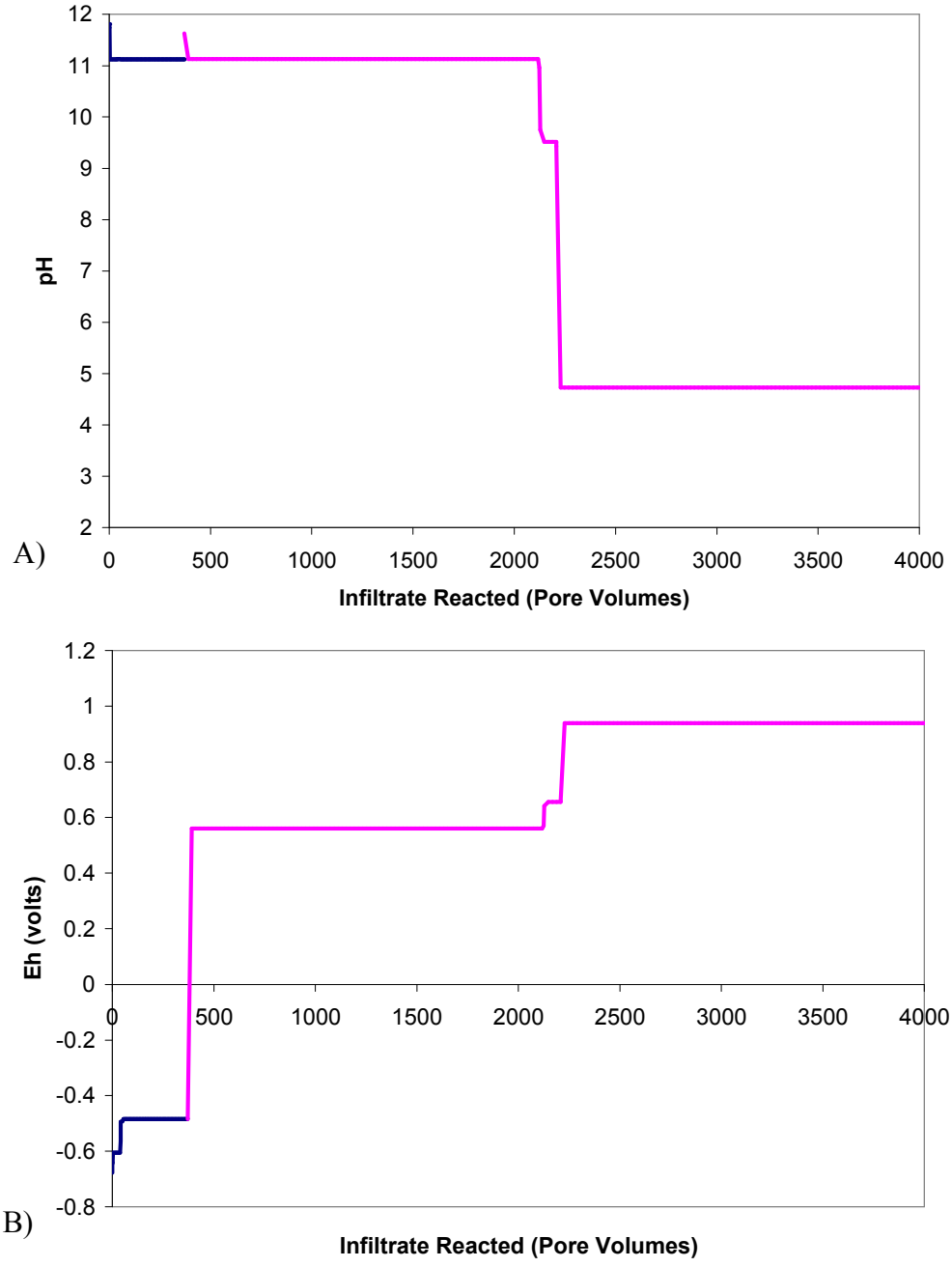


**Figure 12: Pore fluid pH (A) and Eh (B) during simulated degradation of reduced tank grout of non-submerged tanks.**

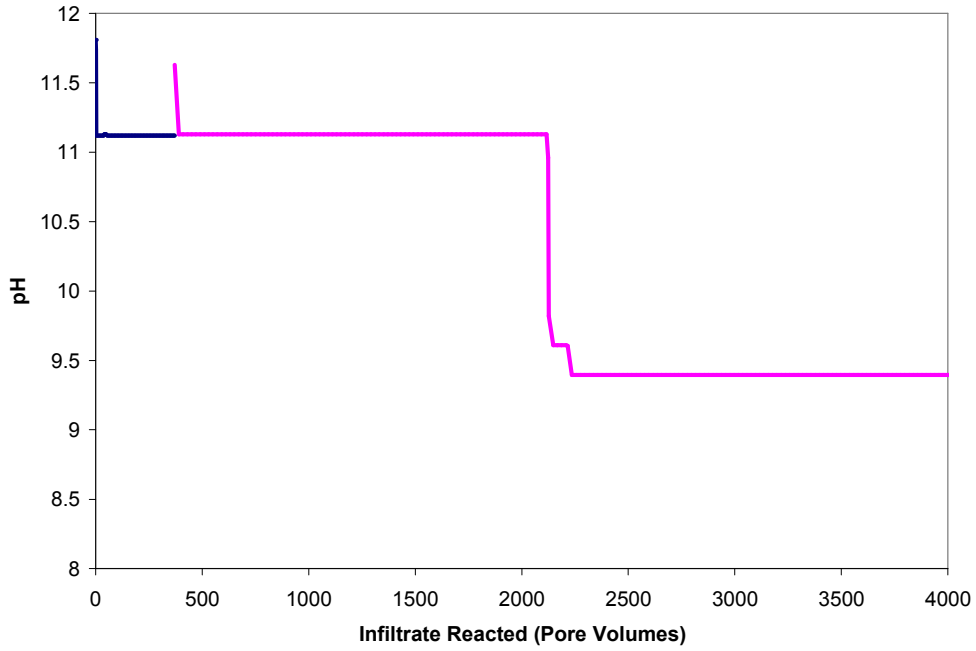


**Figure 13: Pore fluid pH during simulation of reduced grout in non-submerged tanks with hydrotalcite present and allowed to react.**

tanks at pH=9.8 give an indication of what solubilities would be if hydrotalcite were present and allowed to react.

The evolution of Eh during degradation of reducing tank grout in the non-submerged tanks begins at an Eh of approximately -0.6 volts, that in 39 pore volumes rises to -0.48 volts. The Eh stays constant at -0.48 volts for 371 pore volumes at which point it abruptly increases to +0.56 volts. This occurs when all iron sulfide has been oxidized. The increase in Eh at 2131 pore volumes is the result of the sharp decrease in pH at this point. However, in the solubility calculations the Eh is set by equilibrium with calcite to a value of +0.73.

The evolution of pH and Eh during degradation of reducing grout in the submerged tanks is different because of the different pH and dissolved oxygen concentration of the infiltrate. These are presented in Figure 14. The initial pH of 11.1 lasts for 2383 pore volumes of infiltrate reacted at which point the pH drops to 8.6, indicative of equilibrium with calcite. A pH of 8.3, the equilibrium pH of the infiltrate with calcite alone was used to calculate the solubilities of radionuclides. However, the difference of 0.3 pH units makes little difference to the results.

The Eh begins at -0.67 volts but within 70 pore volumes rises to -0.49 volts. The Eh stays contstant at -0.49 volts for 1414 pore volumes, at which point it rises to +0.55 volts. At 2383 pore volumes the Eh rises again to +0.70 volts in response to the pH decrease.

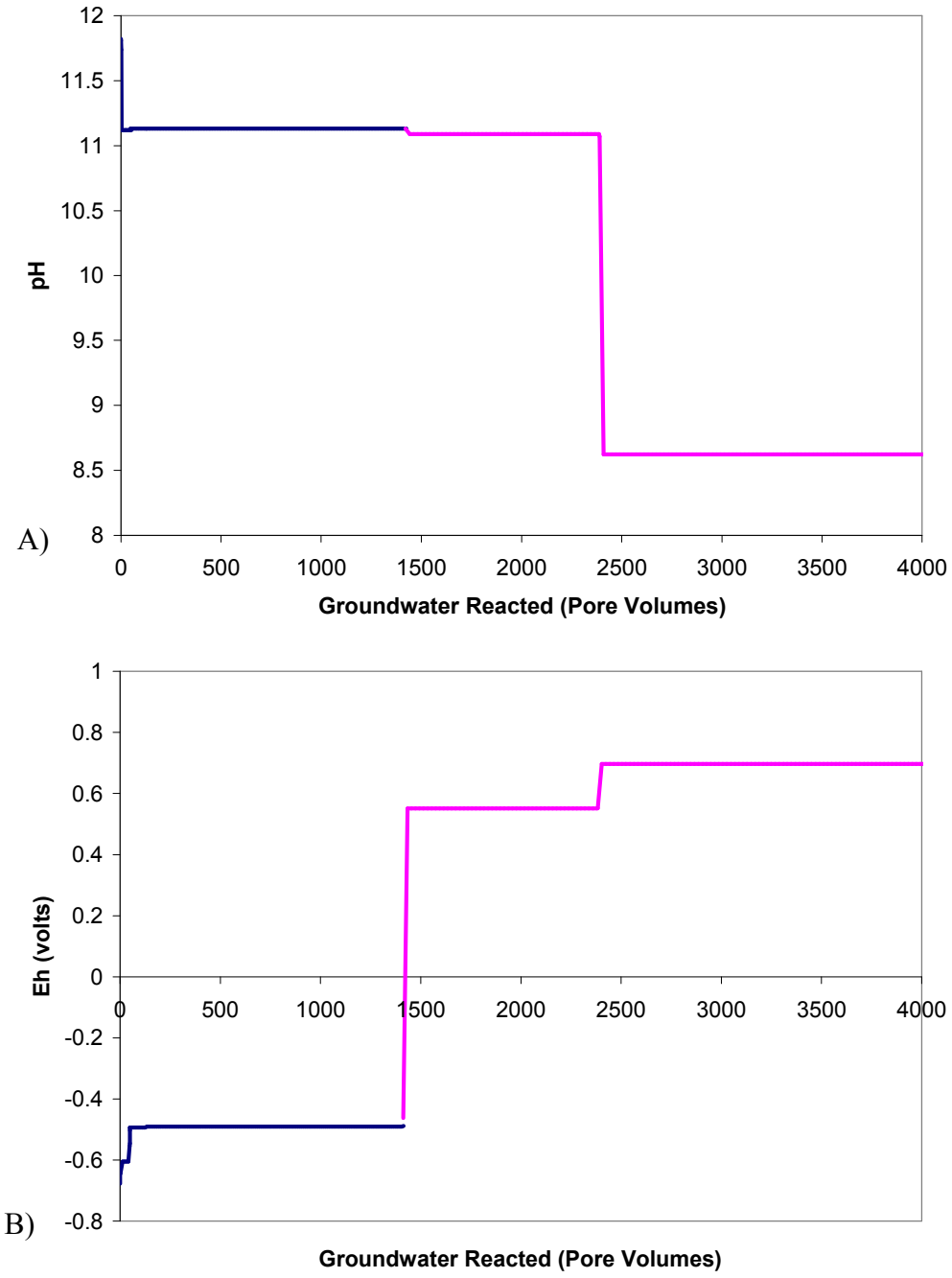


**Figure 14: Pore fluid pH (A) and Eh (B) during simulated degradation of reduced tank grout of submerged tanks.**

*Alternative Grout Mineralogy*

Calculation of normative grout mineralogy from a given chemical composition can be done in different ways that result in different mineralogies. To examine the uncertainty this introduces to radionuclide solubility estimates, different normative mineralogies were calculated. Rather than recalculate all of the solubilities, the change in pH produced by each alternative mineralogy was compared using solubility versus pH diagrams of each radionuclide to observe how the solubility was affected.

Figure 15 shows curves of two alternate normative mineralogies compared to the curve calculated for the original mineralogy in Table 23 The alternate normative mineralogies, shown in Table 27, were calculated assuming that all calcium was in gehlenite or ettringite, rather than CSH. The Geochemist Workbench® recalculates the mineralogy to provide an assemblage that is in equilibrium with the other input parameters prior to beginning the reaction path simulation. For example, all calcium in the original normative mineralogy was put into CSH, but the initial equilibrium calculation by The Geochemist's Workbench® splits calcium between CSH and C4AH13.

**Table 27: Original normative mineralogy used and two alternate normative mineralogies.**

| Mineral | Original grams/$m^3$ | Alternate 1 (Ettringite) grams/$m^3$ | Alternate 2 (Gehlenite) grams/$m^3$ |
|---|---|---|---|
| CSH | 192583 | - | 326153 |
| Ettringite | - | 121725 | - |
| Gehlenite | - | - | - |
| Brucite | - | - | 11357 |
| Hydrotalcite | 47475 | 47475 | 16242 |
| Gibbsite | 50505 | 42940 | - |
| Pyrrhotite | 967 | 967 | 967 |

The simulations were run in the batch mode because "flush mode", or flow through, simulations become unstable before the major pH transitions occur. The x-axis in Figure 15 is "Equivalent Pore Volumes" which is the total amount of fluid after each increment is added divided by the calculated pore volume of 1 cubic meter of reducing grout. The simulations were run to 24,000 Equivalent Pore Volumes.

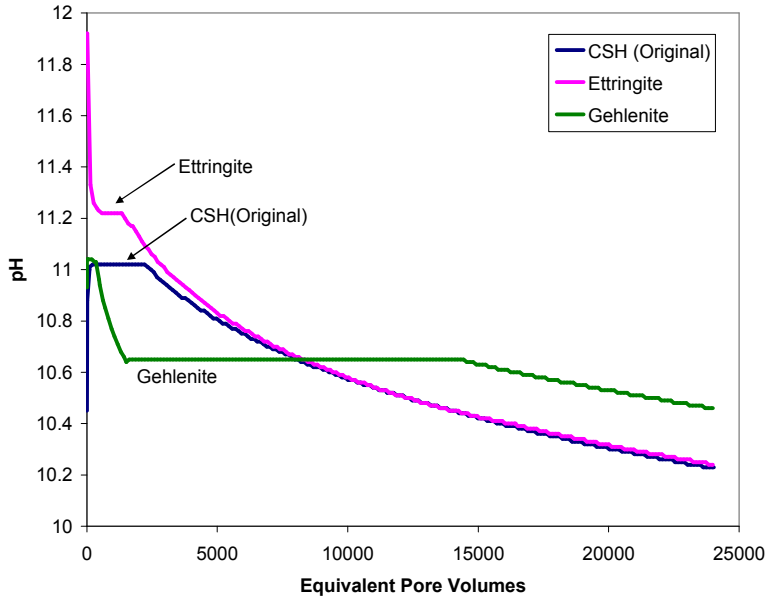


**Figure 15: Comparison of the effect of different normative mineralogies in Table 27 on pH versus Equivalent Pore Volumes.**

In the original simulations – CSH (Original) – the pH is buffered at slightly above 11 for 2102 equivalent pore volumes and then decreases slowly down to 10.2 at 24,000 equivalent pore volumes. When all calcium is put in ettringite, the pH is buffered at 11.2 for 1465 equivalent pore volumes, then decreases along a path nearly identical to the original simulation. When all calcium is initially put in gehlenite, the pH is buffered near 11 for a short time (348 equivalent pore volumes), decreases to near 10.6, and remains there for 14,447 equivalent pore volumes. The plateaus between pH 11 and 11.2 in both alternate mineralogy simulations are the result of CSH controlling pH. Though all calcium was put into ettringite or gehlenite by the normative mineralogy, The Geochemist's Workbench® divided the calcium between CSH and the two initial minerals when it recalculated the equilibrium mineralogy.

Over 5,000 equivalent pore volumes of reacted infiltrate, the pH varies from 11.2 to 10.6 regardless of the mineralogy used. This is consistent with measurements of equilibrium pH of minerals likely to control cement pH in the degradation stage after alkali hydroxides have leached out (Atkins et al., 1992b; Bennett et al., 1992).

As mentioned earlier, the normative mineralogy method of Atkins et al (1992a) is not applicable to the calcium-poor reducing tank grout. Regardless, this method was applied to see if it would make a difference to this sensitivity analysis. Only the first two steps – apportionment of all MgO to hydrotalcite and all $SO_3$ to ettringite can be completed. Thus, the remaining calcium was accounted for by CSH, the remaining $Al_2O_3$ by gibbsite, and the remaining silica by quartz. This produced the normative mineralogy in Table 28. Note the similarity between this mineralogy and that of Alternative 1 in Table 27. No simulations of grout degradation were run with the mineralogy in Table 28, because of this similarity.

**Table 28: Normative mineralogy of proposed reducing tank grout calculated partially by the method of Atkins et al. (1992a).**

| Mineral | Concentration ($g/m^3$ grout) |
|---|---|
| Hydrotalcite | 47209 |
| Ettringite | 121878 |
| CSH | 113031 |
| Gibbsite | 42988 |
| Quartz | 118518 |
| Pyrrhotite | 967 |
| Inert (added quartz sand) | 1369900 |

*Mineralogy Effect on Solubility*

Solubility values of radionuclides under Region II conditions can be affected by the choice of mineralogy because pH will be different. In fact, the solubilities of most radionuclides decrease or remain the same as pH decreases from 11.1 to 10.6 – the range caused by the alternative mineralogies used in Figure 15. Under Reducing Region II conditions 5 elements increase in solubility – Am, Ba, C, Cm, and Sr. Under Oxidizing Region II conditions four elements increase in solubility – Am, Cm, Se, and Sr.

Figure 16 illustrates the range in Am solubility over the pH range of 10.6 to 11.2. The solubility ranges a little over half an order of magnitude. Many radionuclides decrease in solubility as pH decreases from 11.2 to 10.6 because hydroxyl complexes make them more soluble at pH=11.2. Figure 17 shows this effect on the solubility of plutonium. It is assumed that under Region III conditions pH is always controlled by calcite and doesn't vary with initial mineralogy.

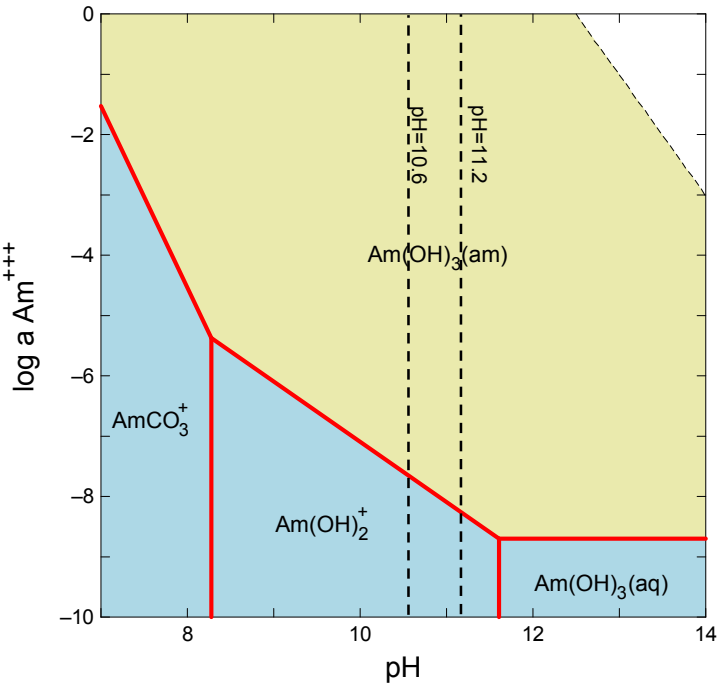


**Figure 16: Americium solubility diagram calculated for Oxidizing Region II conditions using The Geochemist's Workbench® (Bethke, 2005).**

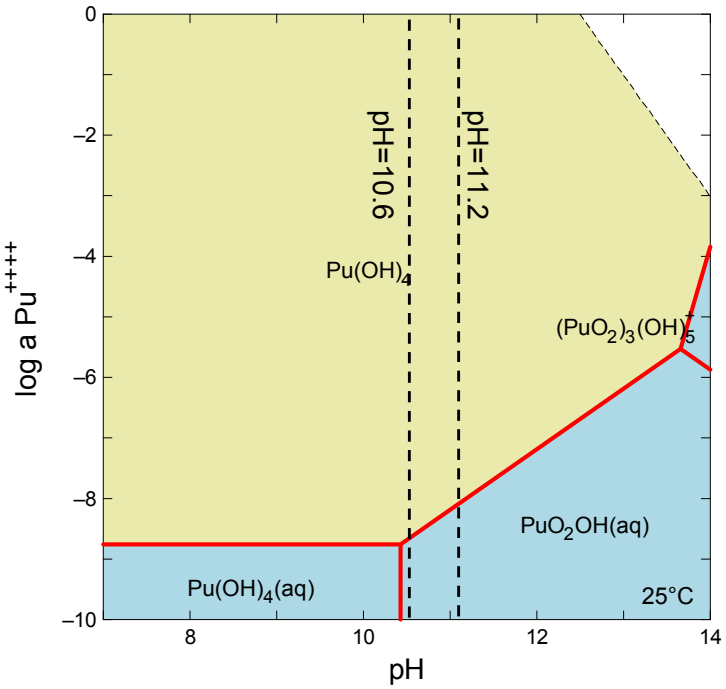


**Figure 17: Plutonium solubility diagram calculated at Oxidizing Region II conditions using The Geochemist's Workbench® (Bethke, 2005).**

Apparent solubilities of U, Pu, and Tc co-precipitated with iron minerals are also affected by changes in pH. Table 29 shows the solubilities of hematite and magnetite, the assumed carrier phases, recalculated based on pH ranges that might occur using a different normative mineralogy. The solubility of hematite and magnetite under Region II conditions decreases as pH decreases because ferric and ferrous iron form aqueous hydroxyl complexes that become more stable as pH increases. Under Oxidized Region III conditions the calculated solubility of hematite remains essentially unchanged over the pH range of 7.5 to 9. The apparent solubilities of U, Pu, and Tc are directly proportional to the solubility of the carrier phase. Thus, the calculated apparent solubilities of co-precipitated U, Pu, and Tc at pH=12.4 are higher than those calculated at lower pH values for Region II conditions and are unchanged over the pH range of 7.5 to 9 under Oxidized Region III conditions.

**Table 29: Solubility of carrier phases hematite and magnetite at pH values of 12.4, 11, and 10.5 at Oxidized Region II, Reduced Region II, and Oxidized Region III conditions.**

| | | Solubility (moles/liter) | | |
|---|---|---|---|---|
| **Condition** | **Carrier Mineral** | **pH=12.4** | **pH=11.0** | **pH=10.5** |
| Oxidized Reg. II | Hematite | $7.5 \times 10^{-10}$ | $3.2 \times 10^{-11}$ | $4.1 \times 10^{-12}$ |
| Reduced Reg. II | Magnetite | $7.8 \times 10^{-8}$ | $3.1 \times 10^{-8}$ | $7.0 \times 10^{-8}$ |
| | | **pH=7.5** | **pH=8.2** | **pH=9.0** |
| Oxidized Reg. III | Hematite | $1.2 \times 10^{-12}$ | $1.2 \times 10^{-12}$ | $1.5 \times 10^{-12}$ |

Hence, use of a different normative mineralogy would make little difference to most of the calculated solubilities reported in this report.

*Alternate Grout formulation*

In addition to these simulations, degradation of an alternate formula of grout was simulated to test the sensitivity of Eh and pH evolution to grout formula. The alternate grout formula is presented in Table 30. The batch runs (Figure 18) show that the number of pore volumes required to bring about major transitions in Eh are linearly related to the amount of slag in the formula, but the Eh is identical during the various stages of grout degradation.

**Table 30: Alternate reducing grout formula used in comparison simulations.**

| Grout Component | Amount (lbs/yd$^3$) | Weight % |
|---|---|---|
| Portland Cement | 300 | 8.71 |
| Class F Fly Ash | 800 | 23.23 |
| Slag | 310 | 9.00 |
| Quartz Sand | 1470 | 42.68 |
| Water | 564 | 16.38 |

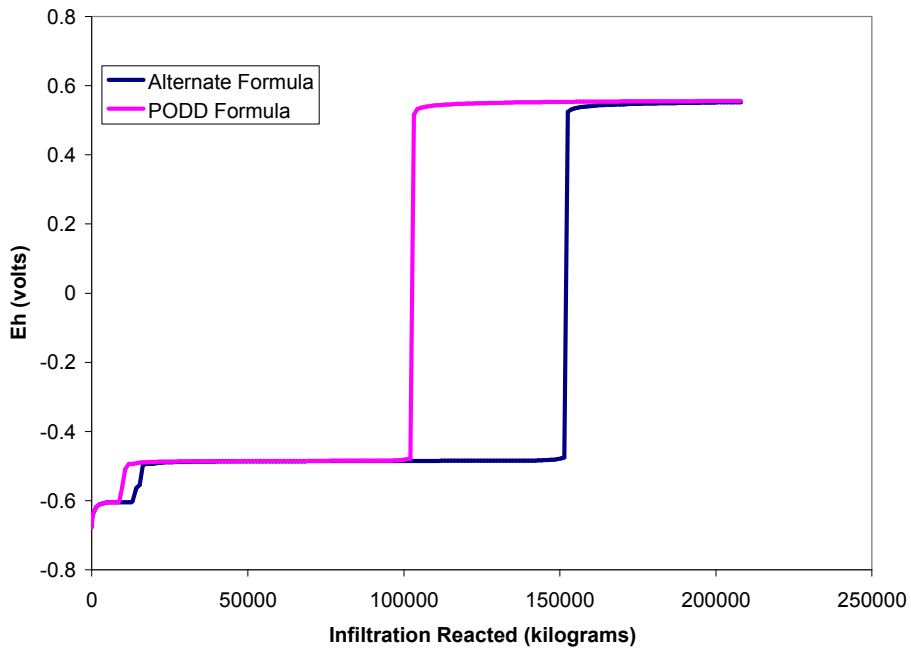


**Figure 18: Eh degradation curve for an alternate grout formulation compared to the formulation used to calculate solubilities in Tables 4 and 5.**

# Appendix C – Comparison of Hanford Tank Characterization and SRS F-Area Tank Characterization

The main text of this document cites observations of Hanford residual tank waste to support arguments about Savannah River Site residual tank waste. Thus, it is useful to compare the residual waste chemistry of the two sites to see if they are similar and to see whether similar processes of waste release might occur. Some differences between washed and unwashed tanks become evident during this comparison and are discussed relative to arguments made in the main text of this document.

The processes used to extract plutonium and recycle uranium at Hanford and Savannah River Site were similar and produced similar waste. There were differences, for example Hanford used the Bismuth phosphate process from 1945 through 1956 and the Redox process from 1952 through 1956. But Hanford also used the Purex process from 1956 through 1972 and again from 1983 through 1988. This was the same process used at the Savannah River Site. The waste generated by these processes was treated in a similar manner. The pH was raised by NaOH to near 14 and there were various volume reduction campaigns, such as evaporation, at both sites.

Compositions of the residual sludges in tanks at both sites are similar suggesting that chemical reactions that produced the sludges are likely to have been similar as well. Table 31 shows concentrations of three major components of the residual waste as well as U-238 and Tc-99 analyzed in samples from five tanks at SRS and five tanks at Hanford.

Concentrations of the major components are all in a similar range and the residual waste at both sites was in contact with high pH supernate dominated by NaOH for long periods of time. Given the observation of co-precipitation of Tc-99 (Cantrell et al., 2006; Krupka et al., 2009) with iron minerals in residual waste at Hanford, it is reasonable to assume that Tc-99 that remains in residual waste after extensive washing at Savannah River Site is also co-precipitated with iron minerals. This is also consistent with the study of Wakoff and Nagy (2004).

**Table 31: Concentrations of some key elements and radionuclides in Savannah River Site and Hanford waste tanks.**

| Tank | Fe (wt.%) | Al (wt. %) | Na (wt.%) | U-238 (mg/kg) | Tc-99 (uCi/g) | Reference |
|---|---|---|---|---|---|---|
| Savannah River Site Tanks | | | | | | |
| 5 | 37.3 | 1.6 | 4.3 | 95500 | 0.013 | Hay et al. (2007) |
| 17 | 24.0 | 3.9 | 9.5 | 10000 | 0.5 | Hay (1997) |
| 18 | 10.4 | 13.4 | 4.7 | 34500 | 0.1 | Swingle (2003) |
| 19 | 2.2 | 12.4 | 16.1 | 2000 | 0.1 | Swingle (2002) |
| 20 | 7.9 | 3.0 | 27.8 | 1800 | 0.9 | d-Entremont and Hester (1997) |
| Hanford Tanks | | | | | | |
| C-103 | 1.2 | 13.6 | 0.8 | 3730 | $3.9 \times 10^{-3}$ | Krupka et al. (2009) |
| C-106 | 3.7 | 8.2 | 4.7 | 310 | 0.024 | Krupka et al. (2009) |
| 202 | 12.2 | 1.4 | 5.9 | 207000 | $2.5 \times 10^{-3}$ | Krupka et al. (2009) |
| C-203 | 1.6 | <0.07 | 9.6 | 505000 | $1.6 \times 10^{-3}$ | Krupka et al. (2009) |
| S-112 | 0.2 | 29.1 | 4.9 | 24 | $8.1 \times 10^{-3}$ | Krupka et al. (2009) |

*Washed and Unwashed Residual Waste*

The waste release model presented in this document assumes the tanks will be cleaned as thoroughly as possible prior to closure and that any soluble Tc-99, or other radionuclides, will be removed by this cleaning. The effects of even mild cleaning may be seen by comparing the water leachable Tc-99 and U in Hanford tank C-106 to Hanford Tanks C-203 and C-204. The residual waste in Tank C-106 was washed with a 0.9 M oxalic acid solution prior to sample characterization by Deutsch et al. (2005). In the post-washing residual waste from this tank 2 to 3.5% of the Tc-99 and 1.3 to 4% of the U was water leachable. This contrasts with the results from tanks C-203 and C-204 reported in Cantrell et al. (2006). These tanks were not washed

prior to sampling the residual waste. For tank C-203, 80% of the Tc-99 and 72% of the U was water leachable from the residual waste. For tank C-204, 25% of the Tc-99 and 82% of the U was water leachable. Thus, radionuclides remaining after washing will be in recalcitrant forms that are difficult to dissolve. This is supported by the results of Hay et al. (2007). In an oxalic acid washing experiment on residual waste from Savannah River Site tank 5, 98% of the U was removed. It is reasonable to assume that the remaining 2% must be in an insoluble form.

Waste release in washed and unwashed tanks is not comparable. For example, the results of Cantrell et al. (2006) for U are not comparable to the waste release model presented in this document. The samples used by Cantrell et al. (2006) are from unwashed tanks and most of the U is water leachable. Cantrell et al. (2006) suggests that poorly crystalline $Na_2U_2O_7$ controls U release after the water soluble U is removed. This is probably true for some of the remaining U – particularly the 27% (C-203) and 14% (C-204) removed by the acetate buffer. But, the 7.3% (C-203) and 8.7% (C-204) removed by the 8M $HNO_3$ extraction may well be co-precipitated with iron or aluminum phases, as this is the stated purpose of this extraction. This residual fraction is what is considered in the waste release model presented in the main text of this document, because it is assumed the SRS tanks will be washed thoroughly.